

UCSF

UC San Francisco Electronic Theses and Dissertations

Title

Nanostructured Surfaces for Drug Delivery and Anti-Fibrosis

Permalink

<https://escholarship.org/uc/item/6bp5n5xb>

Author

Kam, Kimberly Renee

Publication Date

2012

Peer reviewed|Thesis/dissertation

Nanostructured Surfaces for Drug Delivery and Anti-Fibrosis

by

Kimberly Renee Kam

DISSERTATION

Submitted in partial satisfaction of the requirements for the degree of

DOCTOR OF PHILOSOPHY

in

Bioengineering

in the

GRADUATE DIVISION

of the

UNIVERSITY OF CALIFORNIA, SAN FRANCISCO

AND

UNIVERSITY OF CALIFORNIA, BERKELEY

ACKNOWLEDGEMENTS

Thank you to my advisor, Professor Tejal Desai, for her encouragement, guidance, and scientific expertise. I am eternally grateful to her for allowing me to join her lab, nurturing my scientific curiosity, and being so supportive of my interests.

To Professor Song Li and Professor Susana Ortiz-Urda, for serving on my committee and providing guidance with this dissertation.

To Laura Walsh, for her scientific expertise with this project. Laura, you made my time in lab so much fun!

To Dr. Russell Ross, Dr. Jeremy Ollerenshaw, and Suzanne Bock from Kimberly Clark Corporation and Professor Michael Koval from Emory University for their help and support throughout the project.

To everyone in the Desai Laboratory, for being incredibly welcoming and contributing to such a happy and productive work environment. It made me excited to come into lab each day.

To Homayoun Moslehi for his expertise in stratified epithelial models.

To Lily Peng, for being such a wonderful friend and always supporting and looking out for me.

To my parents for their love and support over the past 27 years and for encouraging me to follow my interests and passions.

To my sisters, Natalie and Michelle for being such wonderful role models to look up to.

And last but not least, to my fiancé, Vince, for your love, encouragement, and patience- especially when all I could talk about were nanostructures.

Funding for this work was kindly provided by Kimberly Clark and the National Institute of Health. Immunofluorescence images for these studies were acquired at the Nikon Imaging Center at UCSF. All SEM was performed at the Electron Microscope Laboratory at UC Berkeley

ABSTRACT

Nanostructured Surfaces for Drug Delivery and Anti-Fibrosis

By

Kimberly Renee Kam

Joint Doctor of Philosophy in Bioengineering

University of California, San Francisco

University of California, Berkeley

Professor Tejal A. Desai, Dissertation Committee Chair

Effective and cost-efficient healthcare is at the forefront of public discussion; on both personal and policy levels, technologies that improve therapeutic efficacy without the use of painful hypodermic needle injections or the use of harsh chemicals would prove beneficial to patients. Nanostructured surfaces as structure-mediated permeability enhancers introduce a potentially revolutionary approach to the field of drug delivery. Parental administration routes have been the mainstay technologies for delivering biologics because these therapeutics are too large to permeate epithelial barriers. However, there is a significant patient dislike for hypodermic needles resulting in reduced patient compliance and poor therapeutic results. We present an alternative strategy to harness the body's naturally occurring biological processes and transport mechanisms to enhance the drug transport of biologics across the epithelium. Our strategy offers a paradigm shift from traditional biochemical drug delivery vehicles by using nanotopography to loosen the epithelial barrier.

Herein, we demonstrate that nanotopographical cues can be used to enable biologics > 66 kDa to be transported across epithelial monolayers by increasing paracellular transport. When placed in contact with epithelial cells, nanostructured films significantly increase the transport of albumin, IgG, and a model therapeutic, etanercept. Our work highlights the potential to use drug delivery systems which incorporate nanotopographical cues to increase the transport of biologics across epithelial tissue.

Furthermore, we describe current advancements in nano- and microfabrication for applications in anti-fibrosis and wound healing. Influencing cellular responses to biomaterials is crucial in the field of tissue engineering and regenerative medicine. Since cells are surrounded by extracellular matrix features that are on the nanoscale, identifying nanostructures for imparting desirable cellular function could greatly impact the field. Due to the rise in micro and nanofabrication techniques borrowed from the advances in the microelectronics industry, previously unattainable nanostructured surfaces on a variety of biomaterials can be generated. We investigated how nanostructured surfaces with varying nanofeature aspect ratios can influence fibrosis. Thus, nanostructured surfaces show substantial progress for therapeutic applications in drug delivery and wound healing.

TABLE OF CONTENTS

Chapter 1: Introduction	1
1.1 Nano- and Microfabrication for overcoming drug delivery challenges	8
1.2 Nanofabrication for tissue engineering applications	16
Chapter 2: Nanostructured Surfaces for Loosening the Epithelial Barrier Function	21
2.2 Background	21
2.3 Methods	23
2.4 Results	26
2.5 Discussion	35
Chapter 3: Nanostructured Microneedles as a Drug Delivery Device	40
3.1 Background	40
3.2 Methods	41
3.3 Results & Discussion	43
Chapter 4: Nanostructured surfaces as an Anti-Fibrotic Environment	49
4.1 Background	49
4.2 Methods	51
4.3 Results	55
4.4 Discussion	62
References	67

LIST OF FIGURES

Figure 1	3
Figure 2	5
Figure 3	14
Figure 4	15
Figure 5	18
Figure 6	27
Figure 7	29
Figure 8	30
Figure 9	32
Figure 10	34
Figure 11	43
Figure 12	47
Figure 13	56
Figure 14	57
Figure 15	58
Figure 16	59

Figure 17 _____ 60

Figure 18 _____ 62

CHAPTER 1:

Introduction

Current advancements in the microelectronics industry have led to the creation of new nano and micro materials. These developments have laid the foundation for novel design possibilities that have been applied to biomedical needs. In contrast to traditional techniques, these fabrication methods allow for a higher level of design control that were never before possible. The microelectronics industry provides fabrication methods capable of providing nanometer structures in a wide variety of materials at high throughputs. These materials are fabricated using either "bottom up" or "top down" approaches. In "bottom up" methods, new materials are created from basic molecular components governed by thermodynamics and self-assembly principles. This method is limited by large variations in size, shape, surface charge and chemical composition. In contrast however, the "top down" method is a subtractive process from bulk starting materials and employs specialized microelectronics fabrication techniques. In this review article, we discuss how nano- and microfabrication techniques allow for a high level of design control for therapeutic delivery devices and for tissue engineering.

Precise Nano- and Microfabrication

In the microelectronics industry, a precise pattern of metal lines, holes, or dopant atoms are created on a silicon wafer to generate an integrated circuit. Similarly, this general process can be applied to pattern a wide range of biocompatible materials for medical applications. It is a versatile and facile process that can be employed for the

preparation of drug delivery devices. Conventional photolithography can produce surfaces with ordered structures such as pillars, pits, wells, and grooves at micrometer length scales. It offers a high level of control over the sizes and shapes of drug devices. This method is a combination of three major unit process steps: 1) thin film deposition, 2) photolithography, and 3) etching as shown in Figure 1¹. In the first step, a two dimensional layout of the features is designed using computer aided design (CAD) software and then printed onto a photomask template. Next, the pattern is transferred onto a substrate through photolithography. This technique exposes a photosensitive polymer to UV light according to the design of the photomask. After exposure, the resist is developed to leave a relief pattern on the substrate. Resists can be either positive or negative and depend on whether the radiation exposure hardens or softens the resist's reaction to the developer. Finally, the resulting pattern which is not covered by the photoresist layer is etched anisotropically or isotropically using wet or dry chemical etching processes. A schematic of the general processes is shown in Figure 1. Microfabrication is a powerful tool to develop micron scaled features, but standard photolithography is limited by the wavelength of light and is only capable of generating features with a lower resolution limit between $0.5-1 \mu\text{m}^2$.

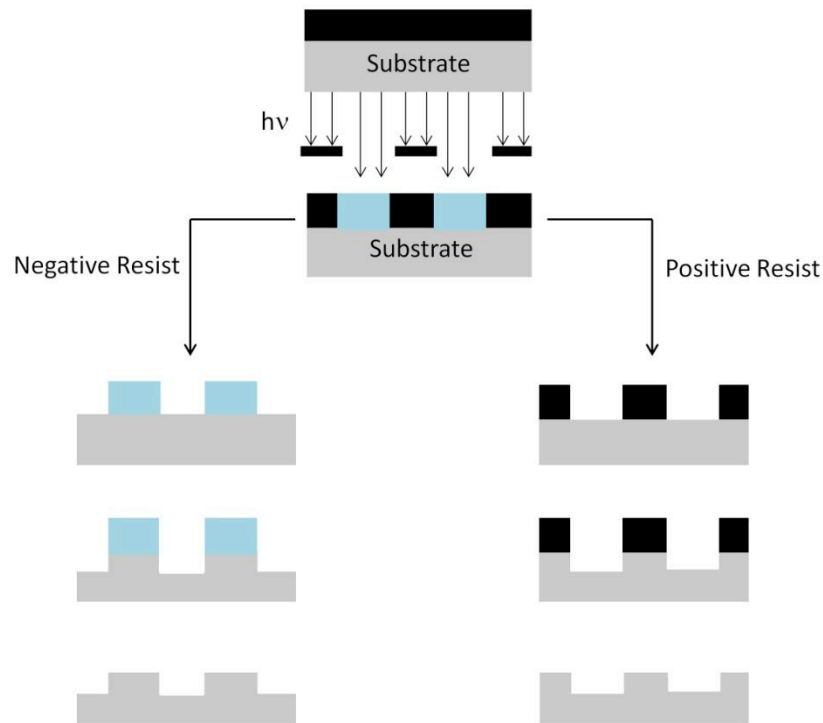


Figure 1| A schematic representation of conventional photolithography with negative or positive photoresist. A substrate, usually made of silicon, is exposed through a mask to generate the pattern. Depending on whether the photoresist is negative or positive, the photoresist is developed to remove soluble regions, and then etching is used to transfer the pattern into the underlying substrate. Reproduced from ⁴⁴.

Other techniques such as electron beam lithography followed by nanoimprint lithography are

capable of generating nanofeatures that are not limited by the diffraction limit of light.

This technique is a stamping process capable of generating nanometer scale patterns as small as 10 to 25 nm and was developed by Chou et al. in the 1990's^{3,4}. In contrast to conventional photolithography, nanofeatures are generated by the direct mechanical deformation of a thermoplastic material using a mold with nanofeatures. The molds are

fabricated using electron-beam lithography as shown in Figure 2. Specifically, a polymer resist material such as PMMA is spin casted onto a silicon wafer. The electron beam rasters across the resist according to the pattern that is programmed into the computer. After developing away the unreacted resist material, reactive ion etching is employed to anisotropically etch the underlying silicon wafer. Using plasma ignited by an RF signal, ions bombard the underlying silicon through chemical and physical etching to generate a mold for NIL. Next, the nano-featured mold is brought into contact with a thermoplastic material, and the temperature is raised above the glass transition temperature while the pressure is raised above the elastic modulus of the material to transfer the nano pattern as shown in Figure 3. This stamping process allows for rapid patterning of larger areas and is low-cost since it does not require specialized equipment. These nanoimprint lithography techniques can be integrated into drug delivery devices or stand alone as devices in themselves.

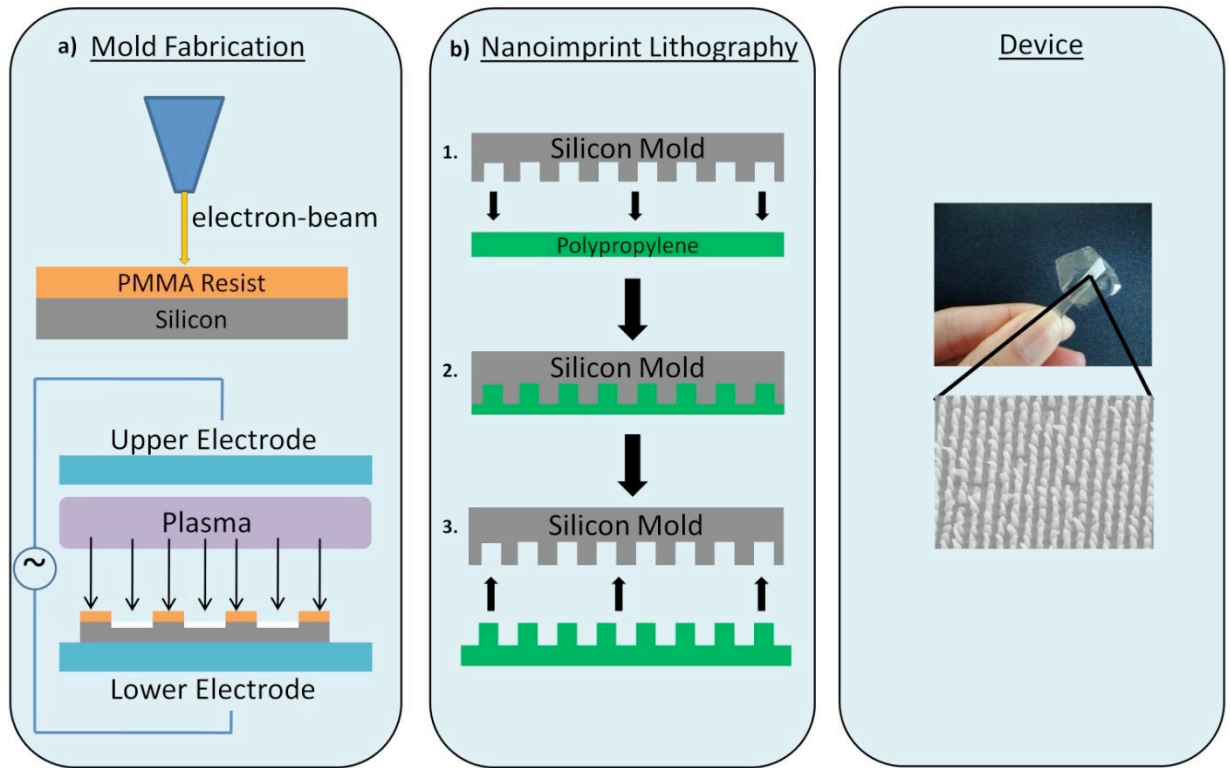


Figure 2| a) Silicon molds for NIL can be fabricated using electron beam lithography to beat the diffraction limit of the wavelength of light. Reactive ion etching is then used to anisotropically etch the underlying silicon wafer. At the end of this process, a silicon mold is generated that is used for the stamping. b) The first step in NIL is to bring the mold in contact with the thermoplastic polymer thin film (for example, polypropylene). The temperature is increased above the T_g of the material and the pressure is increased above the elastic modulus of the polymer to transfer the nano pattern to the thin film.

Additionally, another method involves patterning chemical molecules onto a surface using an elastomeric mold or stamp which is typically made from poly(dimethylsiloxane)⁵. This technique is referred to as nano- or microcontact printing (nCP or μ CP), depending on the stamp feature sizes. The molecules are coated onto a rigid stamp before contacting the substrate. Although this process is attractive because of the low-cost of fabricating the stamp, it is limited by the material distortion during

contact with the substrate. In both μ CP and nCP, imprinting is limited by the reliability of the stamp and the defects from the fabrication process⁶.

Other "top-down" methods include shaping spherical microparticles or nanoparticles into various geometries as payloads for drug delivery. For example, DeSimone's group recently developed a method called Particle Replication In Non-wetting Templates (PRINT)⁷. This technique is capable of fabricating monodisperse particles with precise control over the structure, geometry, and moduli of the resulting particles⁸. Another method reported by Champion and Mitragotri employs spherical particles as starting materials and manipulates the morphologies to generate non-spherical particles. This technique consists of embedding the polystyrene spheres in a polymer film before stretching the film to create ellipsoidal particles. Through this technique, they were able to produce twenty different three dimensional shapes with 200 nm polystyrene spheres as the starting material⁹. Clearly, there is a plethora of nano- and microfabrication techniques to precisely design and prepare drug delivery devices.

CHALLENGES TO DRUG DELIVERY

Tight Junctions and Cell Membranes

There are many challenges to delivering therapeutic agents, ranging from physiological properties of the tissue to physicochemical properties of the drug as outlined in Figure 3. Within the physiological category, the hydrophobic membranes of cells form a highly impermeable barrier to most polar and charged molecules. The plasma membrane is composed of a fluid mosaic of tightly packed lipid molecules interspersed with proteins that are in specific conformations for structural support¹⁰. This selectively

permeable membrane presents a physical barrier to drug absorption and limits absorption to specific routes and mechanisms.

In addition, the barrier function of the epithelia has important implications for drug delivery. Epithelial tissues compartmentalize the body into cavities and are composed of specialized cells that are sealed together by tight junctions in the intercellular space. The paracellular pathway around the cells is one of the main routes for drug diffusion. However, the tight junction pores are small and are approximately 0.5-2 nm, while the hydrodynamic volumes of conventional therapeutics range from few to several hundred nanometers¹¹. Therefore, the tight junctions are a major barrier to drug delivery, particularly for large molecular weight therapeutics¹². In order to deliver large molecules systemically, hypodermic needle injections are administered which have several disadvantages including: low patient compliance, accidental needle-sticks, and the associated medical personnel costs.

Mucosal Layer

Drugs that are delivered through mucosal epithelia such as respiratory and alimentary tracts, encounter a mucosal membrane that acts as a significant barrier to drug penetration. Mucus is composed of long, entangled glycoprotein molecules called mucins that are arranged in a block copolymer-like structure of branched and un-branched blocks. They serve as a lubricant and protective layer for the body. Mucous is composed of 95% water, 4% mucin, and 1% inorganic salts, carbohydrates and lipids¹³. The viscoelasticity of mucus acts as a mechanical barrier to drug passage. Penetrating this

layer would be beneficial to the delivery of drugs across mucosal tissues such as gastrointestinal tract, buccal, vaginal, or lung routes for example.

Clearance

Many drug delivery devices are plagued by the short residence times that they have in contact with the underlying absorption surfaces¹⁴. For example, in the respiratory tract, mucus is involved in the process of mucociliary clearance. In this process, mucus entraps substances (dust and microorganisms), within a viscoelastic mucus layer. It is then propelled by the cilia towards the throat and the particulates are swallowed¹⁰. Although this is a beneficial process for hazardous substances, drug delivery devices are cleared in this way. Additionally, in the gastrointestinal tract, the residence time is affected by the peristaltic environment which leads to rapid clearance. Therefore, increasing the residence times for devices is essential for improving drug delivery.

1.1 Nano- and Microfabrication for overcoming drug delivery challenges

There have been numerous papers that have reported biochemical approaches to mucosal adhesion using agents such as lectins and chitosan^{15,16}. These chemicals have shown to be effective, but they are limited by batch-to-batch repeatability and are expensive to incorporate into a device. Recently however, a new area in bioadhesion has emerged which relies purely on nanostructural and geometrical cues. This structure-mediated approach is an elegant solution to improve the drug residence time in contact with the epithelium, particularly with mucosal tissue. Specifically, a chemical vapor deposition (CVD) method was reported in which silicon nanowires were grown from

silica microbeads (30-50 μm in diameter)¹⁷⁻¹⁹. It was observed that these fabricated devices significantly increased bioadhesion to mucosal tissues *in vitro* and *in vivo*. Nanowires were also shown to upregulate the mRNA expression levels of PKC which regulates the tight junctions by controlling the contraction of the acto-myosin filaments. Therefore, these nanostructures induced cellular restructuring via mechanotransduction pathways by interacting with cells at previously unattainable length scales as supported by the morphological changes in tight junction proteins (ZO-1 and Claudin 1)¹⁷. Therefore, these nanoengineered microparticles were able to loosen the tight junctions and significantly enhance bioadhesion, thereby increasing the residence time for model drugs¹⁷.

Others have investigated how gecko-inspired nanostructures can increase adhesion to tissues. Geckos stick to a variety of surfaces through their hierarchically structured foot pads, which are finger-like spatulas made of beta-keratin. They adhere to surfaces because of their high surface area to volume ratio of nanosized spatulae, which together adhere to surfaces arising from weak secondary bond forces called van der Waals forces²⁰. Although most of the research has investigated dry adhesion, Izadi et al. has developed nonsticky fluoropolymer films that have exhibited remarkable adhesion in both dry and wet conditions due to van der Waals forces, electrostatic attractions, and hydrophobic effects²¹. Lee et al. has also developed a reversible adhesive material that is effective in both wet and dry environments²². They fabricated a regular nanopillar array on a substrate material of poly(dimethyl-siloxane) (PDMS) elastomer using electron-beam lithography. Combined with a mussel-mimetic polymer layer, the device was able to reversibly adhere under wet conditions. In another report, a biocompatible and

biodegradable elastomeric material was used for fabricating gecko-inspired adhesives using a silicon template made from photolithography and reactive ion etching. The polymer was cast into the mold and cured by UV light to create nanoscale pillars. Like all micro and nanofabrication techniques, this method was highly controlled and tunable, allowing them to systematically vary the dimension of the nanoscale pillars. They investigated the ratio of the tip diameter to pitch distance to determine the parameters that lead to enhanced wet tissue adhesion²³. These gecko-inspired fabrication techniques are novel approaches that could be applied to drug delivery devices for enhancing the drug residence time by improving adhesion to mucosal tissues.

A strategy to overcome the challenge of fast clearance has been addressed by a number of different groups. For example, Adriani et al. recently reported the fabrication of mesoporous nanoparticles in disk-like and rod-like shapes to improve particle adhesion under microvascular shear flow conditions²⁴. The mesoporous nanoparticles were fabricated using a three-step process consisting of 1) porosification of the silicon film through electrochemical etching, 2) photolithography to pattern the film, and 3) reactive ion etching to form particles. They discovered that the intermediate sized disk-like particles and the largest rod-shaped particles adhered the strongest compared to other sizes. This microfabrication strategy of precisely tuning the size and shape of particles to enhance adhesion could have significant benefits for drug delivery by increasing the drug residence time with the epithelium.

Another innovative strategy to overcome the barrier function of the epithelium, and in particular stratified epithelium, is through the use of microneedles. Microneedles pierce the skin in a non-invasive and painless way. They penetrate the outer 10-20 μ m of

the skin, creating shunts to the dermis for delivering drugs topically or systemically. Microneedles are fabricated with a wide range of materials and are typically fabricated as an array of up to hundreds of microneedles over a substrate. The first microneedles were produced from silicon wafers by photolithography followed by deep reactive ion etching²⁵. Other production methods have recently been developed for creating less expensive and biocompatible materials such as metal, polymer, and sugar-based microneedles. Metal microneedles are mainly produced through laser cutting from sheet metal and bending them perpendicularly out-of-plane. Polymeric microneedles can be biocompatible and because of their viscoelastic properties, they are less prone to breakage once in the skin²⁶. Drugs can also be incorporated into biodegradable polymeric microneedles for controlled delivery.

Microneedles have proven effective throughout the literature. While many groups have reported how microneedles enhance the permeability of low and high molecular weight compounds^{27,28}, recent papers have also found microneedles to be effective for vaccine delivery. In one recent study by Matsuo et al., a dissolving hyaluronate microneedle array was used as a transcutaneous immunization device to improve protective immune responses for vaccine antigens²⁹. There have also been reports on improving upon the traditional design of microneedles. For example, Chu et al. recently investigated separable arrowhead microneedles, which is a novel approach to the current limitations of polymer and metal microneedles³⁰. The arrowhead tips contain encapsulated drug and immediately separate from the metal needle shaft once inserted into the skin. This strategy allows for a quick, safe, and self-administered therapy as an alternative to hypodermic needle injections. The metal shafts provide strong mechanical

integrity which allows for skin insertion, and the detachable arrowhead tips eliminate biohazardous sharp waste enabled by dissolving microneedles. Therefore, microfabrication has enabled the systemic design of microneedle arrays in order to overcome the barrier of stratified epithelium for transdermal drug delivery.

Microfabrication enables the rational design of nano and microparticles with different shapes and geometries in order to probe the cell membrane barrier. The shape of the particle influences a number of behaviors associated with drug delivery. For example, recent studies have reported that particles of various non-spherical geometries influence the rates of cellular internalization. In one study, HeLa cells were reported to internalize nonspherical particles made by PRINT processing that resemble rod-like bacteria with dimensions as large as $3 \mu\text{m}^3$ ³¹. However, other studies by this group showed that cubic particles with lengths of 3-5 μm were not internalized. They reported how the particles with higher aspect ratios seemed to exhibit higher internalization rates than the lower aspect ratio cubic particles. However, it appears that aspect ratios that are too high have greater difficulty being internalized by macrophages. Studies by Geng et al. and Sharma et al. reported that particles with aspect ratios greater than 23 exhibited reduced phagocytosis, and studies by Champion et al. also show that aspect ratios greater than 20 are not phagocytosed^{9,32,33}. The observed trends in particle aspect ratio could be explained by the thermodynamic and kinetic modeling and analyses reported by Li et al.³⁴. They constructed an endocytosis phase diagram of radius versus particle aspect ratio for the conscious design of drug delivery nanoparticles. In this paper, Li et al. reported that the optimal nanoparticle radius for the fastest endocytosis rate is 25 nm. This minimum radius decreases as the aspect ratio increases which would explain the

empirical results from the studies by Geng et al., Sharma et al., and Champion et al..

In other studies, nano and microtopographical cues were discovered to modulate cellular internalization rates. For example, Teo et al. cultured mesenchymal stem cells and monkey kidney fibroblasts on nano and micropillar substrates that were fabricated with electron beam lithography followed by nanoimprint lithography³⁵. After FACS analysis, they reported higher cellular internalization of fluorescently labeled dextran when cells were cultured on the micron sized pillars. They hypothesized that these larger pillars were able to induce more actin-dense regions compared to the smaller nanopillars. This phenomenon would translate into higher intracellular contractility, upregulation of Rho GTPases, and higher rates of macropinocytosis.

Furthermore, another advantage of microfabrication is that it is capable of creating microdevices with precisely controlled modular components that are tailorable for specific drug delivery applications. For example, Bernards et al. recently reported a novel fabrication method to create nanoporous thin films for the zero-order release of a small molecule and protein³⁶. The theory behind this approach is that the nanopores were made to be on the same length scale as the drug of interest so that single-file, concentration-independent transport was achieved. Bernards et al. grew zinc oxide rods hydrothermally and used the resulting nanorods as a template. They then spin casted a solution of biodegradable polycaprolactone onto the nanostructured template. After etching away the ZnO in a weakly acidic solution, a nanoporous PCL thin film was achieved. Others have reported similar nanoporous membranes fabricated through different methods. For example, nanoporous PCL thin membranes were fabricated for zero-order drug release of IFN- α , an antitumor agent. This group recently reported a hot

embossing technique followed by phase inversion to create nanoporous membranes with pores of approximately 20-60 nm³⁷. These nanofabrication methods allow for controlled nano-pore sizes to achieve zero-order drug release.

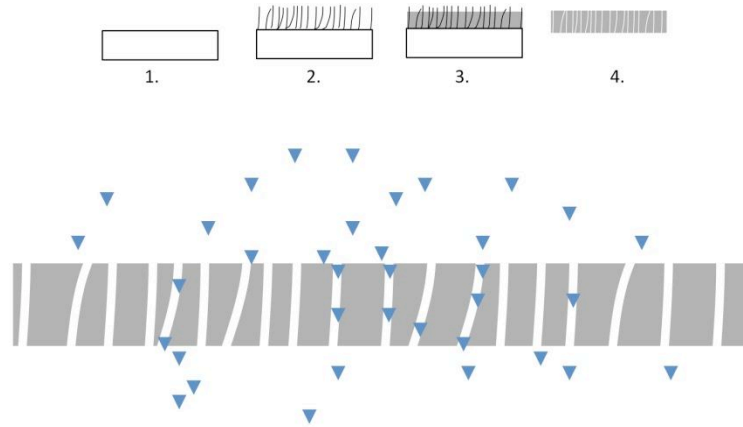


Figure 3| Zinc oxide nanowires were grown hydrothermally on an underlying substrate and served as a template. Afterwards, a thin layer of polycaprolactone was spin casted onto the nanowires. The nanowires were then etched away, resulting in a nanoporous membrane. The nanopores allow for single-file linear diffusion across the nanoporous membrane.

Microfabrication has also been reported in the development of devices for overcoming the drug targeting and adhesion barriers in gastrointestinal drug delivery. For example, Ainslie et al. developed a device for the asymmetric delivery of chemotherapeutics from microfabricated patches made by photolithography techniques. The micropatch device consisted of a protected drug reservoir that concentrated the chemotherapeutic in a hydrogel which has advantages over traditional spherical particles. The planar patch geometry allows for unidirectional concentration gradients unlike the radial concentration gradients from spherical particles. This reduces the necessary

therapeutic volume and subsequently decreases drug toxicity to neighboring tissues. Finally, the microfabrication methods allow for a controlled ways to load multiple therapeutic agents by successive spin-coating and photolithography steps.

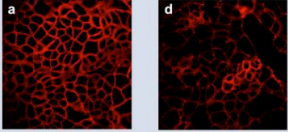
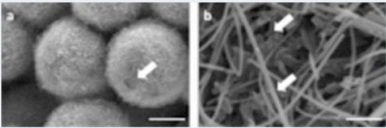
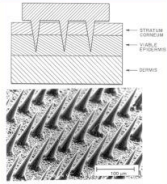
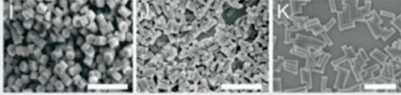
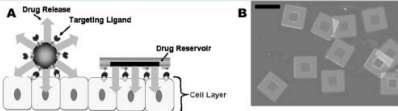
Specific Challenge	Nano or Micro Fabrication Solution	Examples
a. Tight junctions seal epithelial cells together (0.5-2 nm in width)	<ul style="list-style-type: none"> Nanowires loosen the tight junctions (ZO-1 and Claudin 1) for paracellular drug delivery 	 <p>Control Nanowires</p>
b. Device adhesion	<ul style="list-style-type: none"> Nanowires increase van der Waals forces Gecko-inspired wet adhesive materials 	
c. Overcoming the stratum corneum barrier for transdermal drug delivery	<ul style="list-style-type: none"> Microneedles provide shunts to the dermis, disrupting the dead corneocytes, for topical or systemic drug delivery 	
d. Controlling cellular internalization	<ul style="list-style-type: none"> Micro or nanoparticle geometry, shape, & surface chemistry influences endocytosis 	
e. Achieving therapeutic drug concentrations	<ul style="list-style-type: none"> Planar microdevice for unidirectional concentration gradients 	

Figure 4| An outline of the various drug delivery challenges that are overcome by nano and microfabrication. a) Claudin-1 tight junction fluorescence has a higher intensity and a greater thickness in the control monolayer compared to when the epithelial monolayer was incubated with nanowires¹⁷. b) Nanowires lead to higher bioadhesion due to the higher surface area to volume ratios for higher van der Waals interactions¹⁸. c) Microneedles penetrate the skin and disrupt the stratum corneum in transdermal drug delivery⁵⁰. d) Nanoparticles of varying geometries lead to differences in cellular internalization rates³¹. e) Planar devices contribute to asymmetric concentration gradients for enhanced therapeutic delivery¹.

1.2 Nanofabrication for tissue engineering applications

In addition to drug delivery device applications, nano- and microfabrication techniques have enabled new strategies for regenerating injured tissues. The goal of tissue engineering is to restore function by delivering cells, biological factors, and a biomaterial scaffold for cells to adhere, organize, and develop into native tissue. For many wounds, the "repair" mechanism is more dominant compared to the "regeneration" mechanism, and as a result, scar tissue is formed instead of well-oriented tissue. With the rise in nano- and microtechnology, researchers now have the tools to recapitulate the submicron architecture of the extracellular matrix. These different nano- and microtechnologies enable researchers to begin understanding the cell-material interactions at the nanoscale and to better influence desired cellular behaviors.

One novel strategy for tissue engineering is the fabrication of nanofibers to mimic the fibril architecture of the extracellular matrix. ECM contains many biological fibrils that have diameters ranging from tens of nanometers to micrometers in scale³⁸. They serve as not only structural support, but also as a guide for tissue morphogenesis, cellular differentiation, and tissue remodeling. Nanofibers can be fabricated by electrospinning strategies, one of the most promising techniques for designing 3D-scaffolds for tissue engineering applications. It uses an electrical charge to draw very fine (micro to nano scale) fibers from a liquid. There has been much evidence in the literature that nanofibers can be used as tissue engineering scaffolds to accelerate wound healing in dermal substitutes, blood vessel regeneration, and nerve repair³⁹⁻⁴¹. As an example, in a report by Kurpinski et al., epidermal skin cell migration was observed to be significantly higher when the nanofibers were aligned compared to when they were unaligned. They reported

that the aligned nanofibers allowed for the cells to more easily penetrate the scaffold. These results demonstrate the importance of biophysical properties and extracellular matrix architecture on cell infiltration⁴². In another study by the same group, bi-layer nanofibrous nerve conduits were fabricated where the luminal layer had longitudinally aligned fibers to guide nerve regeneration and the outer layer had randomly organized fibers for structural support. They showed *in vivo* that the alignment was superior to the random nanofibrous conduits. These different studies on nanofibers strongly support the argument that fibril architecture on the nanoscale is critical to tissue regeneration⁴³.

Controlled interactions of cells on biomaterial substrates is a critical prerequisite for tissue engineering approaches. It is hypothesized that the *in vivo* nano-architecture of the ECM contributes to these cellular behaviors. One technique in particular, nanoimprint lithography, has enabled researchers to understand the connection between cellular behavior and surface geometry, roughness, and feature size in a systematic way⁴⁴. It is a promising method for exploring tissue engineering and integrates both high resolution with high throughput at a low cost. In one study by Yim et al., grated substrates made from NIL resulted in more elongated smooth muscle cells compared to non-imprinted substrates⁴⁵. Similarly, multiple-layers of nanograted tissue culture polystyrene were formed by successive nanoimprinting to form a 3D scaffold *in vitro*. The nanogratings, ranging from 350 nm to 10 μ m, led to significantly higher cell elongation and alignment of bovine pulmonary artery smooth muscle cells⁴⁶. Additionally, nerve cells grew on top rather than inside nano-patterned grooves (100-400 nm wide) made from NIL as seen in Figure 4⁴⁷. Therefore, NIL has proven to be a powerful method that is capable of coaxing

seeded cells to orient in specific ways and may eventually lead to therapeutic applications in vivo.

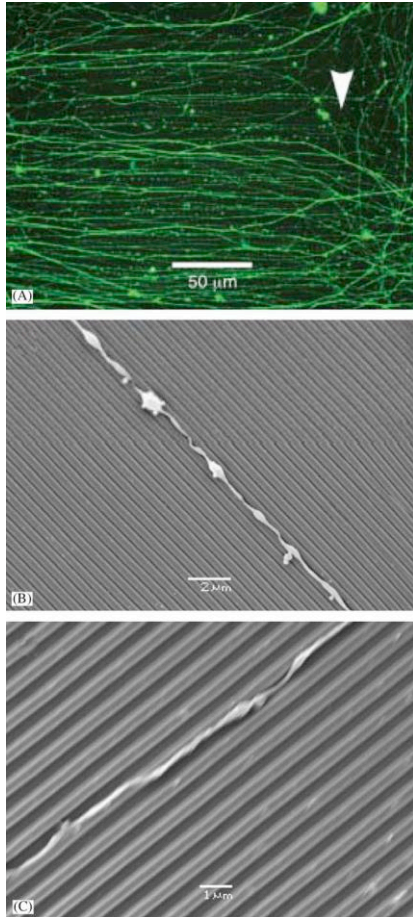


Figure 5| a) Axons are clearly aligned with the imprinted pattern (200 nm width and 400 nm pitch) compared to the unimprinted regions where the axons exhibit more random growth (the arrow indicates the border of the nanoimprinted pattern). b) (100 nm width and 500 nm pitch). c) (400 nm width and 800 nm pitch). The axons grow on the top of the ridges and not in the grooves. Taken from ⁴⁷

Other nanostructured strategies have reported to have differential effects on various cell types. For example, surfaces treated with ionic plasma deposition result in a high degree of surface roughness on the nano length scale. Nanorough surfaces are desirable to achieve improved osteoblast function and decreased fibroblast functions, thus decreasing scar formation. In a study by Cohen et al., the high degree of nano-roughness prevented fibroblasts from attaching to the implant material and proliferating⁴⁸. In

addition, a study by Peng et al. also showed that titanium nanotubes led to significantly enhanced endothelial cell proliferation and decreased smooth muscle cell proliferation, as an application for decreasing restenosis in stent devices⁴⁹. This strategy of using nanostructures to have differential effects on cell types could be applied to other tissue engineering studies as well.

Future directions

The new field of nano and microfabrication research has considerable room for growth and offers exciting new therapeutic applications. Nano- and microfabrication will continue to be investigated for therapeutic applications because of the ability to combine modular components such as shape, geometry, and size into a single device. Future work may include a further understanding of how the device influences specific biological processes on the nano- and microscale that could be harnessed for drug delivery and tissue engineering applications. This would enable the exploration of a spectrum of subtle interactions that were previously unattainable.

Although this field has demonstrated promising results so far, it's important to recognize that it is still in its infancy. Most studies have been performed in only *in vitro* models. *In vivo* considerations such as biodistribution, toxicity, protein adsorption, wound healing responses, and device removal have had limited exploration. Furthermore, until recently, research in the area of cellular responses to nano- and microtopography have been limited to qualifying morphological parameters such as alignment, area, and elongation. However, a major limitation in this area of research has been the lack of controllable and definable chemistries, protein adsorption, and adhesion. However, as the

barrier between biology and engineering decreases, these areas will soon be addressed. Therefore, the field of nano- and microfabrication research has considerable room for growth and offers exciting possibilities for the future of drug delivery and tissue engineering.

CHAPTER 2:

Nanostructured Surfaces for Loosening the Epithelial Barrier Function

The tight junctions of epithelial cells present a major obstacle to drug delivery which limits absorption of molecules greater than 0.5 - 20 kDa. We present a novel platform composed of nanostructured polymer surfaces that enable biologics > 66 kDa to be transported across epithelial monolayers by reversibly increasing paracellular transport through tight junctions. Various nanostructures differed in the ability to enhance permeability. When placed in contact with epithelial cells, the most effective nanostructured surfaces increased transport of albumin, IgG, and etanercept by more than 10-fold. This work highlights, for the first time, the potential to use nanotopographical cues, rather than chemical agents, to increase the transport of biologics.

2.1 BACKGROUND

Although injections have been the mainstay technology for delivering macromolecular therapeutics, bolus injections can invoke an immune response leading to poor bioavailability and clinical efficacy. In addition, injections are limited by the patient discomfort and the need for physician oversight which can lead to a lack of compliance. Alternative drug delivery systems have been developed to utilize routes through more convenient and accessible tissues, such as the epithelia of the nose, mouth, eye, skin, and gastrointestinal tract¹⁻⁶. However, because the physiological function of the epithelia is to prevent entry of toxins into the body, numerous barriers prevent absorption of larger

molecules. Tight junctions, fast clearance, and charge interactions combine together in different tissues to form barriers that prevent the entry of molecules larger than 20 kDa in the gastrointestinal tract down to 0.5 kDa in the stratum corneum of the skin^{57,58}.

To improve the distribution and absorption of biologics, new delivery techniques need to be developed that enhance clinical efficacy and safety through specific control over drug transport mechanisms in epithelial tissue. Recent studies have shown that micro- and nanostructures can induce cellular restructuring via mechanotransduction pathways by interacting with cells at previously unattainable scales^{31,59–62}. Specifically, in the context of drug delivery systems, it has been shown that structure and geometry play a large role in determining the efficiency of particle uptake by cells^{9,11}. More recently, Fischer et. al demonstrated considerable cytoadhesive properties for drug delivery applications of nanoengineered microparticles with nanowires having dimensions comparable to the size of cellular microvilli¹⁴.

Inspired by this structure-mediated approach to drug delivery, we report for the first time that a therapeutic biologic (etanercept), with a molecular weight of 150 kDa, can be transported across the epithelial barrier without the use of chemical moieties. We demonstrate that the transport enhancement results from interactions between a nanostructured polymer surface and the epithelial cells, reversibly altering transport by utilizing inert mechanical cues. This platform approach to drug delivery is a paradigm shift from traditional biochemical strategies and could greatly impact the field of drug delivery.

2.2 MATERIALS & METHODS

Fabrication of Nanostructured Films

Molds for NIL were generated using the JEOL JBX-9300FS EBL System and selective reactive ion etching. The molds were stamped into FDA-approved polypropylene (Premier Lab Supply Inc., 25.4 mm) and polystyrene thin films (Plastic Suppliers Inc., 50.8 mm). The polymer thin films were placed in contact with the nanostructured molds and exposed to a temperature of 170°C and a pressure above the elastic modulus of the polymer films using an Obducat 6-inch nanoimprint lithography system. Afterwards, the mold was removed, resulting in well-defined nanofeatures.

Cell Culture

Human intestinal Caco-2 cells (American Type Culture Collection (ATCC), Manassas, VA) were cultured in MEM with Earle's BSS supplemented with 20% FBS, 1% penicillin-streptomycin, and 1% sodium pyruvate, in an atmosphere containing 5% CO₂ and 90% relative humidity at 37°C. The cells were subcultured at 90% confluency by trypsinization with 0.05% trypsin-EDTA. Cells from passage numbers between 12 and 18 were used for the experiments.

Transport studies

Caco-2 cells were grown to confluency on Transwell permeable supports (Corning) until tight junctions formed as measured by a transepithelial electrical resistance (TER) value greater than 400 Ohm x cm² (World Precision Instruments). The nanostructured films were placed in contact with the epithelial monolayer barrier. Next, a PBS solution

(Invitrogen) containing either FITC-BSA (Sigma-Aldrich, 66 kDa), FITC-IgG (Sigma-Aldrich, 150 kDa), or etanercept (Immunex Corp., Thousand Oaks, CA, 150 kDa) was introduced to the apical side of the well inserts. The concentration on the basal side of the insert was sampled at different time points and measured with a fluorometer and microBCA assay (Pierce Biotechnology). To test for active transport from tight junction remodeling, the transport studies were conducted at either 4°C or 37°C and were equilibrated at the designated temperature for 30 minutes before commencing.

Transcellular Biochemical Blocking

Etanercept transport studies were performed in the presence of Dynasore to block dynamin-mediated endocytosis transport across the Caco-2 cell monolayer. Dynasore (BioVision) was reconstituted in DMSO at 80 mM and then diluted in MEM- α medium to 80 μ M. After washing the Caco-2 monolayers with PBS, the cells were incubated at 37°C in the presence of the Dynasore solution. Transport studies were performed as described above in the presence of the nanostructured films. To block caveolae endocytosis, caco-2 monolayers were incubated with genistein (200 μ M) for 1 hour at 37°C before performing the transport studies in the presence of the nanostructured surfaces as previously reported⁶³.

Immunofluorescence staining of ZO-1

Cell monolayers from the transport studies were stained for zonula occludens-1 (ZO-1) to visualize the morphology of the tight junctions after contacting the nanostructured surfaces for 2 hours and then at 24 hours after the nanostructured surfaces were removed. Methanol at 4°C was used to fix and permeabilize the cells. The samples

were incubated with a primary antibody (ZO-1 rabbit polyclonal antibody, Invitrogen) solution diluted 1:100 at 25°C for 1 hour. After washing with PBS, a 1:100 secondary antibody solution (Abcam) was added for 1 hour at 25°C. The samples were then mounted for confocal microscopy imaging.

qPCR Studies

Caco2 cells were seeded at a density of 50,000 cells in a 96-well tissue culture plate. P(1.5) or P(flat) surfaces were placed in contact with the cells for 2 hours at 37°C. Cell lysis, reverse transcription (Eppendorf), and qPCR (Applied Biosystems, StepONEPlus) were performed using the Fast SYBR Green kit in accordance with the manufacturer's instructions. The experiment was performed in triplicate (n=3) and the evaluation of mRNA expression by qPCR was also performed in triplicate. The expression of GAPDH (forward 5' CTCTCTGCTCCTCCTGTT CG-3', reverse 5'-GCCCAATACGACCAAATCC-3'), ZO-1 (forward 5'-TGTGAGTCCTTCAGCTGTGG-3', and reverse 5'-TTTCCTGCTCAACTCCTTCG-3'), ocln (forward 5'-ACCGAATCATTATGCACCAAGC-3', reverse 5'-AGATGGCAATGCACATCA CAA-3'), MLCK (forward 5'-CCCGAGGTTGTCTGGTTCAAA-3', reverse 5'-GCAGGTGTA CT TGGCATCGT-3'), and FAK (forward 5'-GGCCTGCTTTGGATTCCG C-3', reverse 5'-CAGTGAACCTCCTCTGACCG-3') were analyzed. The results from the real time PCR were analyzed using the $\Delta\Delta C_t$ method and normalized to GAPDH transcript levels.

Statistical analysis

Data are reported as mean values +/- standard deviation. Multiple comparisons were analyzed with a one-way ANOVA test followed by the Holm t-test. P-values of less than 0.05 were considered statistically significant

2.3 RESULTS

Fabrication of nanostructured surfaces

Four distinct categories of nanostructured surfaces were fabricated through nanoimprint lithography and injection molding as presented in Figure 6: a polypropylene film with nanopillars (average height, $H = 300$ nm, average diameter, $D = 200$ nm, aspect ratio (AR) = 1.5, surface roughness = 47nm); a polypropylene film with higher aspect ratio nanopillars ($H = 16$ μ m, $D = 800$ nm, AR = 20, surface roughness = 850 nm); a polystyrene film with nanopillars ($H = 1$ μ m, $D = 200$ nm, AR = 5, surface roughness = 73 nm); and finally, a polystyrene film with 3 different nanopillars combined in a fractal pattern with the largest pillar diameter of 1 μ m having an average height of 520 nm, the medium pillar diameter of 400 nm having an average height of 560 nm, and the smallest pillar diameter of 200 nm having an average height of 680 nm. The AR ratios for the three structures were 0.5, 1.4, and 3.4, and the average surface roughness was 145 nm. All films will be referred to as either P or S for polypropylene or polystyrene respectively, followed by the nanostructure aspect ratio in parentheses (e.g. "P(1.5)" encodes for the polypropylene film with a nanostructure aspect ratio of 1.5).

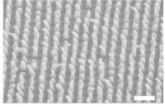
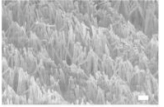
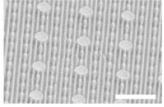
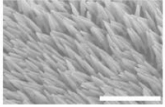
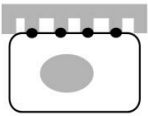
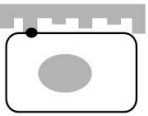
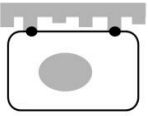
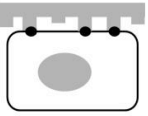
Properties	P(1.5)	P(20)	S(0.5, 1.4, 3.4)	S(5)
				
Surface Roughness	47 nm 	850 nm 	145 nm 	73 nm 
Aspect Ratio	1.5	20	0.5, 1.4, 3.4	5
Shear Modulus	218 MPa	27 MPa	319 MPa	39 MPa

Figure 6| The structure-property relationships of the nanostructured surfaces. Polypropylene nanostructured surfaces are designated by "P" while polystyrene nanostructured surfaces are indicated by "S." The number in parenthesis corresponds to the aspect ratio of the nanofeature as measured by the ratio of the average height to the average diameter. Scale bars for P(1.5) is 400nm while the scale bars for P(20), S(0.5, 1.4, 3.4), and S(5) are all 3 μm. Surface roughness schematics of the nanostructured surface in contact with an epithelial cell represent how increased surface area results in fewer focal contact points (black circles) for integrin-ligand engagement to remodel the tight junctions and decrease the epithelial barrier function.

Drug transport was investigated using confluent monolayers of Caco-2 cells in contact with the nanostructured surfaces. The Caco-2 cell line is a commonly used transport model of the epithelium. Transport studies were performed by first growing a confluent Caco-2 monolayer on Transwell inserts and then placing the nanostructured surface in contact with the already-formed epithelial barrier. This is a significantly different setup than other studies in the literature where epithelial cells are grown directly on the nanostructured surface⁶⁴⁻⁶⁶. Next, a solution of one of the following proteins was introduced onto the apical side of the monolayer: bovine serum albumin conjugated to fluorescein isothiocyanate (FITC-BSA, MW = 66 kDa), immunoglobulin G conjugated to

FITC (FITC-IgG, MW = 150 kDa), or etanercept (MW = 150 kDa). At different time points, the concentration was measured on the basal side of the transwell insert.

The P(1.5) surface, with its relatively low aspect ratio of 1.5 and low surface roughness of 47 nm improved the transport properties the most for all proteins tested in the polypropylene group (Figure 7). The S(0.5, 1.4, 3.4) surface, exhibiting similarly low aspect ratios of 0.5, 1.4, and 3.4 and a surface roughness of 145 nm was the best performing polystyrene surface. Interestingly, the P(20) surface with the highest aspect ratio and surface roughness had the lowest permeability and displayed similar effects on transport as the untreated and unimprinted controls. From the results in Figure 7, it appears that an optimal surface roughness exists in the range of 47-145 nm to disrupt epithelial barrier function and enhance permeability. Additionally, drug transport across the cell monolayer is optimized when the nanostructure aspect ratio ranges from 0.5 to less than 5. These two trends are consistent for both the polypropylene and polystyrene nanostructured surfaces, indicating that the enhanced drug transport is not simply related

to chemical differences and is largely a nanotopographical effect.

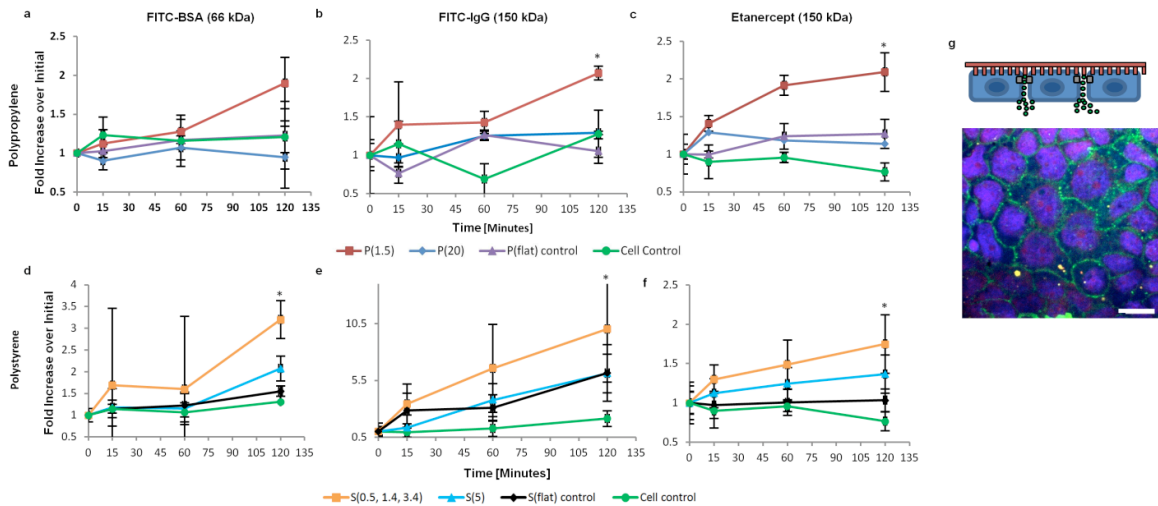


Figure 7| *In vitro* transport studies. Permeability studies show that the nanostructured surfaces with lower aspect ratios and lower surface roughnesses significantly enhance the transport of high MW species across the Caco-2 cell monolayers over 2 hours. Data is displayed as the mean (+/- standard deviation) fold increase over the initial point which is the time when the nanostructured films were placed in contact with the cells. A value of "1" corresponds to no change in drug transport. a, b, and c are the transport of FITC-BSA, FITC-IgG, and etanercept, respectively, across the cell monolayers in contact with the nanostructured polypropylene surfaces. d, e, and f are the transport of BSA-FITC, IgG-FITC, and etanercept, respectively, across the monolayers in contact with the nanostructured polystyrene surfaces. P (1.5) and S(0.5, 1.4, 3.4) induce the highest drug transport for the polypropylene and polystyrene films, respectively. g It appears that the IgG-FITC (green) is located around the Caco-2 cells (blue Hoechst) in the paracellular space. Scale bar is 20 μ m.

Mechanisms for enhancing transport

The enhanced drug transport could be due to different mechanisms that can be broadly classified as either passive or active cellular processes. The nanostructured surfaces could: mechanically disrupt the tight junction proteins that seal cells together, trigger active tight junction remodeling to allow for paracellular transport, and/or invoke transcellular pathways requiring energy-dependent processes. To investigate these

mechanisms, the transport studies were performed at 4°C and 37°C to elucidate whether active processes were at play (Figure 4). When the monolayers were maintained at 37°C, transport was significantly enhanced. However, when the monolayers were maintained at 4°C compared to the physiological temperature (37°C), etanercept transport remained unchanged over 4 hours. Therefore, this study suggests that the nanotopography induces active transport processes through either tight junction remodeling to allow for paracellular transport and/or cellular internalization via transcellular transport.

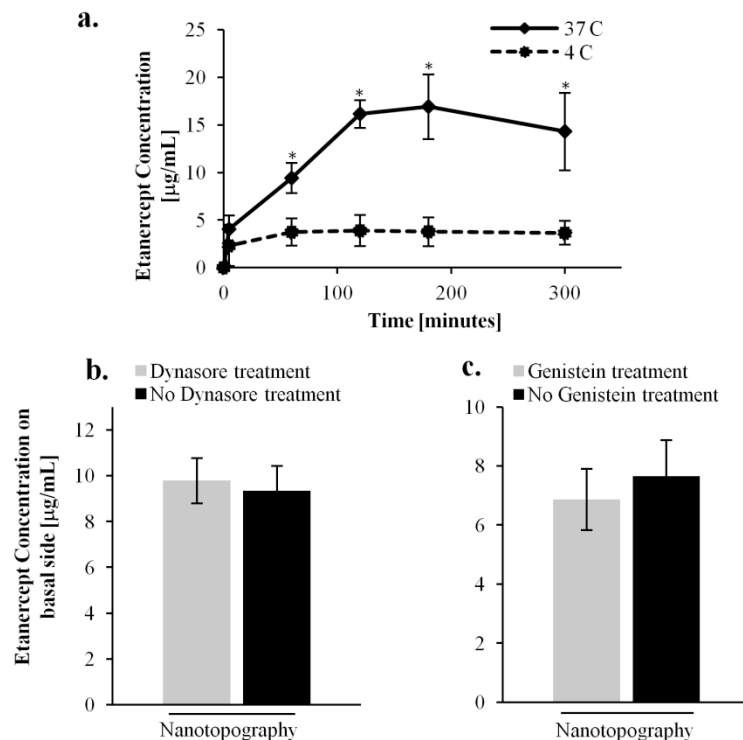


Figure 8| Active transport processes. a Etanercept transport studies performed at 4°C and 37°C show significantly higher transport at the physiological temperature. The transport is retarded at the lower temperature. These results indicate that the enhanced transport is due to active transport instead of passive mechanisms. b Dynasore was used to inhibit dynamin-mediated endocytosis and shows no significant effect on the transport of etanercept across the epithelial monolayer. c Similarly, genistein was used to inhibit caveolae-mediated endocytosis and also does not affect the transport of etanercept.

To further examine this active transport mechanism, different signaling molecules were investigated through gene expression studies. From Figure 5, it is apparent that the P(1.5)

nanostructured surface has a dramatic effect on overall transcription levels. For example, myosin light chain kinase (MLCK), an important regulator of paracellular permeability, increased by 5.6-fold in cells that contacted P(1.5) compared to the controls. MLCK is a protein kinase associated with tight junctions through the contraction of the cortical actin cytoskeleton and has been previously reported to enhance paracellular permeability^{19,20}. These results suggest that the nanotopography increases paracellular transport by inducing mechanotransduction pathways. Additionally, focal adhesion kinase (FAK) transcript expression was examined to measure the formation of focal adhesions as an indication of the level of signaling through integrin binding and clustering. The FAK mRNA expression was increased over 16-fold in cells that contacted the P(1.5) nanostructured surfaces.

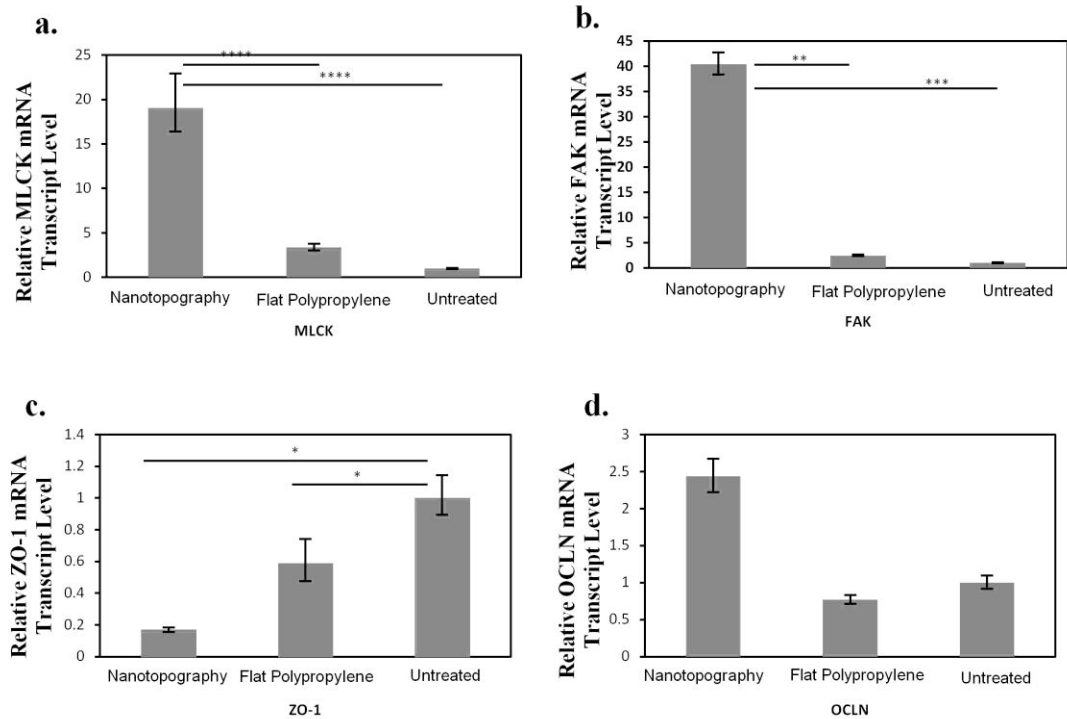


Figure 9 | Quantitative PCR Studies. The gene expression levels of tight junction proteins zonula occludin-1 (ZO-1) and occludin (ocln) are displayed in a and b. The gene expression levels of the signaling molecules, Myosin light chain kinase (MLCK) and focal adhesion kinase (FAK) are also displayed in c and d. Data is normalized by expression levels of each gene by the controls (cells alone) and presented as an average +/- standard deviation. * $p < 0.05$, ** $p < 0.005$, *** $p < .002$, and **** $p < 0.001$, $n = 3$.

Furthermore, we investigated the influence of the nanotopography on the expression of two major protein components of tight junctions by qPCR: zonula occludin-1 (ZO-1) and occludin (ocln). P(flat) controls and P(1.5) nanostructured surfaces were placed in contact with the cells for 2 hours. The tight junction scaffolding protein, ZO-1, exhibited a 3.5-fold decrease in gene expression in cells that contacted P(1.5) in comparison to the cells that only contacted the P(flat) controls. Ocln expression

increased by over 3-fold when cells contacted P(1.5) versus the P(flat) controls (Figure 5).

We further examined whether the nanotopography actively remodels tight junctions to enable paracellular transport by performing immunofluorescence staining of the tight junction protein, ZO-1. The nanostructured surfaces were placed in contact with the cells following the same procedures used in the drug transport experiments. As shown in Figure 8, the cell monolayer that had been in contact with the nanostructured P(1.5) surface for 2 hours exhibited remarkable ZO-1 membrane ruffling in comparison to the control which displays an intact cobblestone morphology. After 2 hours, the nanostructured surfaces were removed, and the monolayers were incubated at 37°C for 24 hours. Within the 24 hours, the ruffled morphology reverted back to the intact tight junction configuration and the TER values recovered which indicates the reversibility of the tight junction remodeling.

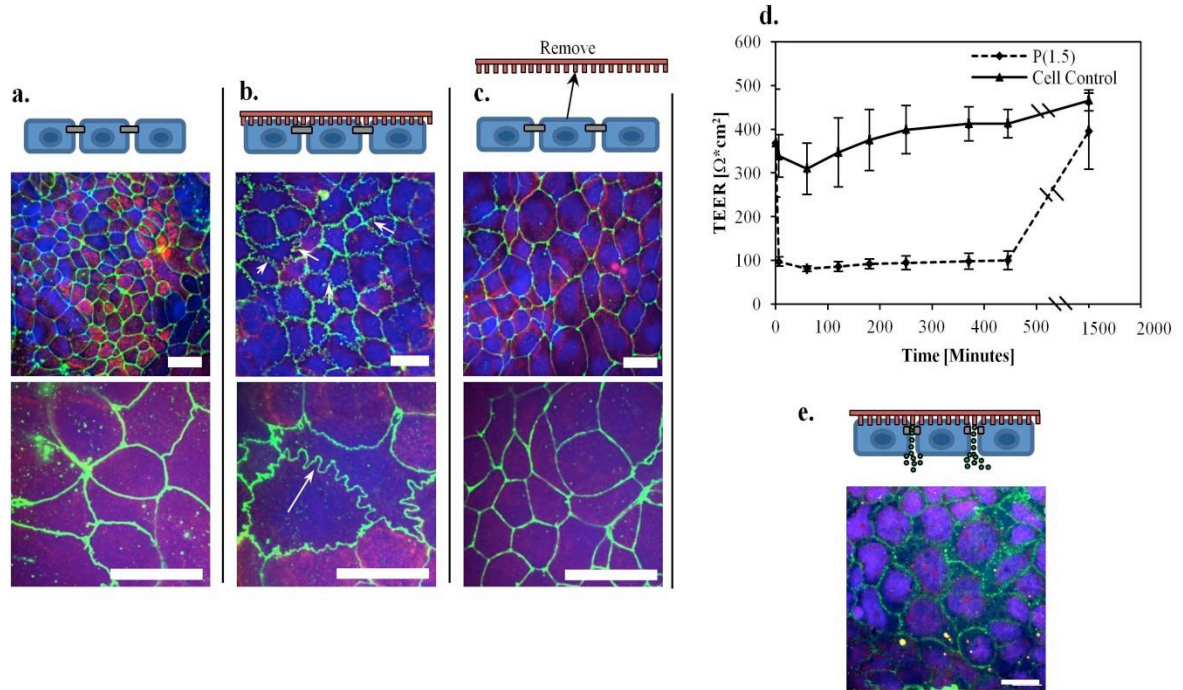


Figure 10| Tight junction morphological changes. Immunofluorescence staining of the tight junction protein, zonula occluden (ZO-1), was performed. **a** Staining of the untreated caco-2 monolayer shows a normal cobblestone morphology. **b** It is apparent that the P(1.5) nanostructured surface induces a dramatic ruffled morphology after 2 hours (see arrows), indicating tight junction remodeling and a loosening of the epithelial barrier to allow for paracellular transport. **c** After P(1.5) was removed from the monolayer and incubated for 24 hours, the ZO-1 morphology reverts back to the normal cobblestone architecture, indicating a reversible rearrangement. **d** TER measurements before and after the nanostructured surface is placed in contact with the cells. TER measurements decreased in the presence of the surface, but eventually increased after 24 hours which demonstrates the reversible and non-deleterious effects of the nanostructures on the cells. Scale bars for the three top images and three bottom images are 10 μm and 20 μm , respectively.

It is clear that paracellular transport is at play, however, we also investigated if the transcellular route contributed to the enhanced transport. Two small molecule endocytosis inhibitors were selected to block transcellular transport. Dynasore, a small molecule inhibitor that blocks the GTPase activity of dynamin, was used to block

dynamin-mediated endocytosis, while genistein was used as a blocker for caveolae endocytosis^{15,21}. The results in Figure 9 show that the inhibitors did not significantly decrease the etanercept transport across the epithelial barrier. Therefore, the transcellular transport pathways related to dynamin and caveolae endocytosis do not significantly contribute to the increased etanercept transport in the presence of the nanotopographical cues.

2.4 DISCUSSION

By screening different nanostructured surfaces, we discovered that high molecular weight drug transport is correlated to two parameters: surface roughness and nanofeature aspect ratio. Nanotopography with a surface roughness between 47-145 nm and nanofeature aspect ratios between 0.5-1.5 induced significantly higher drug transport. It is well established that surface roughness on the nanoscale influences the interface between nanomaterials and different epithelial cell types such as keratinocytes and mammary epithelial cells¹⁶⁻¹⁸. For example, studies have demonstrated that surface roughness on the nanoscale alters cytoskeletal rearrangements and cellular focal adhesions as observed through morphological changes¹⁶⁻¹⁸. These cytoskeletal components, such as F-actin, are tethered directly to tight junction proteins (zonula occludens, claudins, occludin, and junctional adhesion molecules), which are the elements responsible for epithelial barrier function²²⁻²⁵. Therefore, the surface roughness on the nanoscale may influence junction restructuring through physical cues mediated by integrin-ligand engagement and cytoskeletal rearrangements. These mechanotransduction cues may be stronger when the surface roughness is less than 145 nm as we observed. Lower surface roughness promotes higher interfacial area for contact points between the nanostructured surfaces and the

cells. This concept was suggested by our gene expression results. For example, the cells in contact with P(1.5) exhibited significantly higher transcript levels of FAK which supports the theory that the cells interact with the lower surface roughness via integrins. In contrast, the P(20) film with its high surface roughness close to 1 μm , provides a weaker physical interaction with the cells to influence tight junction rearrangement (Figure 6).

With regards to the nanofeature aspect ratio, previous work has demonstrated that silicon nanowires with aspect ratios greater than 16 (length = 3 μm , diameter = 60 nm) tend to collapse over on themselves and mat together, reducing the overall available surface area for cytoadhesion¹⁴. This theory may be implicated for the high aspect ratio P(20) which induced the lowest drug transport. The P(20) higher aspect ratio nanostructures are more compliant and have a lower critical buckling load, which reduces the ability to impart the necessary mechanical stimulus on the cells to remodel the tight junctions. Studies have shown throughout the literature that mechanical stimuli applied to cells via nanotopographical cues invoke numerous cytoskeletal rearrangements through force-induced mechanotransduction pathways^{12, 13, 19, 22}. Therefore, the aspect ratio of the nanofeatures may be another critical parameter to influence the degree of mechanical stimuli on the cells, which ultimately affects the drug transport across the epithelium.

Additionally, our transport studies at 37°C and 4°C indicate that the nanotopography alters the cellular processes related to active transport. At 4°C, the nanostructures do not enhance protein transport, while at 37°C, the transport is significantly higher. These results implicate an active transport mechanism which occurs at the physiological temperature. Therefore, the drug transport enhancement is not due to

a passive, mechanical puncturing of the epithelial barrier. To investigate these active processes, we tested whether the protein was transported across the epithelial barrier via the transcellular or the paracellular pathways.

To do this, inhibitor studies were performed to block endocytosis, and thereby transcellular transport as well. Figure 9 shows that the protein concentration on the basal side is not significantly different with or without the endocytosis inhibitors. This suggests that the nanostructures do not induce transcellular transport related to dynamin or caveolae mediated endocytosis. Instead, the dramatic ruffled morphology of ZO-1 indicates that the tight junction proteins are disrupted and that the paracellular pathway is mainly responsible for the enhanced drug transport. The ZO-1 ruffles appear to be on a length scale that is commensurate to the spacing between the nanopillars of the P(1.5) surface. We hypothesize that the relatively compliant cell membrane snakes around the stiff nanopillars, resulting in the ruffled pattern. Studies by Teo et. al and others demonstrated that topography can alter cellular morphology. Although their setup was different from ours in that they grew cells directly onto the nanostructured surface, they also demonstrated that nanotopography induced membrane ruffling that was coordinated by the actin cytoskeleton²⁶. In the present study, we hypothesize that the membrane curvature induced by the nanopillars may contribute to the loosening of the tight junction barrier through mechanotransduction pathways.

This restructuring of the tight junctions to allow for paracellular drug transport is further supported by the gene expression results. There is a significant decrease in ZO-1 mRNA expression levels compared to the controls as shown in Figure 10. Many studies in the literature have reported that a correlation exists between a decrease in ZO-1 protein

expression and enhanced paracellular permeability. For example, Tian et. al demonstrated that stimulation of HK-2 cells with TGF- β resulted in a decrease in ZO-1 protein expression, indicating tight junction disassembly and a subsequent increase in paracellular permeability²⁷. Similarly, hepatic growth factor (HGF) stimulated RPE monolayers were observed to lose barrier function resulting from a decrease in ZO-1 protein expression in the presence of HGF²⁸. Therefore, a decrease in ZO-1 gene expression is consistent with tight junction disassembly and enhanced paracellular permeability.

We also observed an increase in the expression of occludin (ocln) due to the nanostructured surface. Ocln is a transmembrane component of tight junctions that regulates paracellular permeability. Consistent with our results, Wang et. al also observed an increase in protein expression of ocln and enhanced paracellular permeability when BMECs were treated with VEGF²⁹. Our results suggest that the nanostructures are influencing mechanotransduction pathways to actively remodel the tight junctions and facilitate the paracellular transport of etanercept. Furthermore, this phenomenon appears to be a reversible process as indicated by the TEER values returning to their original values when the nanostructured surfaces are removed after 24 hours. Therefore, the tight junctions are recovering and the nanostructured surfaces do not illicit cytotoxic effects. We have concluded that the nanostructures dramatically affect the paracellular pathway by affecting the tight junction proteins.

CONCLUSION

Our work is the first to demonstrate an enhancement in high molecular weight biologics delivery using nanotopographical cues. We significantly improved the transport of biologics by leveraging the natural biology of cellular processes related to tight junction rearrangements to allow for paracellular transport. By highlighting this enabling strategy of nanostructure-mediated transport, new light will be shed on the field to improve the efficacy and delivery of high potential biologics.

CHAPTER 3:

Nanostructured Microneedles as a Transdermal Drug Delivery Device

3.1 BACKGROUND

The field of microelectronics has enabled the fabrication of nano-scaled geometries for devices in the biomedical industry. One such application of these fabrication techniques is in the production of microneedles for transdermal drug delivery, whereby the drug is delivered into or through the skin for topical or systemic delivery, respectively. The main advantage of microneedles over traditional hypodermic needle injections is that they are relatively short and thin, only penetrating the outer 10-20 μm of the skin. Therefore, they do not reach the underlying dermis and are painless for the patient.

Microneedles are fabricated with a wide range of materials and are typically fabricated as an array of up to hundreds of microneedles over a substrate. The first microneedles were produced from silicon wafers by photolithography followed by deep reactive ion etching²⁵. Other production methods have recently been developed for creating less expensive and biocompatible materials such as metal, polymer, and sugar-based microneedles. Metal microneedles are mainly produced through laser cutting from sheet metal and bending them perpendicularly out-of-plane. Polymeric microneedles can be biocompatible and because of their viscoelastic properties, they are less prone to breakage once in the skin. Drugs can also be incorporated into biodegradable polymeric microneedles for controlled delivery.

Microneedles have proven effective throughout the literature. For example, Mikszta et al. and McAllister et al. reported that the permeability of mouse and rat skin was enhanced by orders of magnitude for low molecular weight compounds up to high molecular weight protein therapeutics^{27,28}. Other studies have reported controlled microneedle coating processes, termed "dip-coating." In one study, a uniform coat of calcein, vitaminB, bovine serum albumin or plasmid DNA was localized just to the microneedle shafts and dissolved within 20 seconds in porcine cadaver skin⁷⁶.

Microfabrication has enabled the systemic design of microneedle arrays in order to overcome the barrier of stratified epithelium. Herein, we report both *in vitro* and *in vivo* transport results from conformally wrapping nanostructured polymer thin films around microneedles. Upon insertion of the nanostructured microneedles into stratified epithelium, a significant increase in drug transport is observed systemically.

3.2 MATERIALS & METHODS

In Vivo Studies

The nanostructured surfaces were integrated into a 25 mm by 25 mm transdermal microneedle patch for *in vivo* drug delivery studies in a rabbit model. Eleven New Zealand White rabbits weighing approximately 4 kg were used, all in healthy condition. Each animal was closely clipped to remove the fur in the left flank region approximating an 8cm x 8cm area. The study consisted of 3 groups: (1) the subcutaneous injection group receiving 2.5 mg/animal (n=2), (2) the P(0.5, 1.4, 3.4) wrapped microneedles group receiving 1.875 mg/animal (n=5), and (3) the unstructured microneedles group receiving 1.875 mg/animal (n=4). The microneedle patches had the nanostructure film conformally

molded over the microneedles using vacuum suction and heat as shown in Figure 11. The *in vivo* test facility used for this animal study is registered with the United States Department of Agriculture to conduct research in laboratory animals and is AAALAC accredited. The study was reviewed and approved by the Facility's Institutional Animal Care and Use Committee (IACUC).

Blood samples were drawn into serum separator tubes from an ear vein for measurement of serum etanercept concentration prior to dosing or patch application as a baseline reading. Serum samples were periodically taken at 30 minutes, 2, 6, 24, 48 and 72 hours. All animals were euthanized following collection of the last blood sample. Blood samples were kept on ice for 30 minutes for separation prior to centrifugation in a refrigerated centrifuge. Serum was aspirated, transferred to clean tubes and immediately frozen and stored in the dark at $\leq -70^{\circ}\text{C}$ until analysis. Etanercept was assayed in duplicate samples from each serum collection using Human sTNF-receptor ELISA kit (R&D Systems, Minneapolis, MN cat# DRT200) which has a minimum detectable dose of 0.6 pg/mL.

Statistical analysis

Data are reported as mean values +/- standard deviation and +/- standard error in Figure 12. Multiple comparisons were analyzed with a one-way ANOVA test followed by the Holm t-test. P-values of less than 0.05 were considered statistically significant

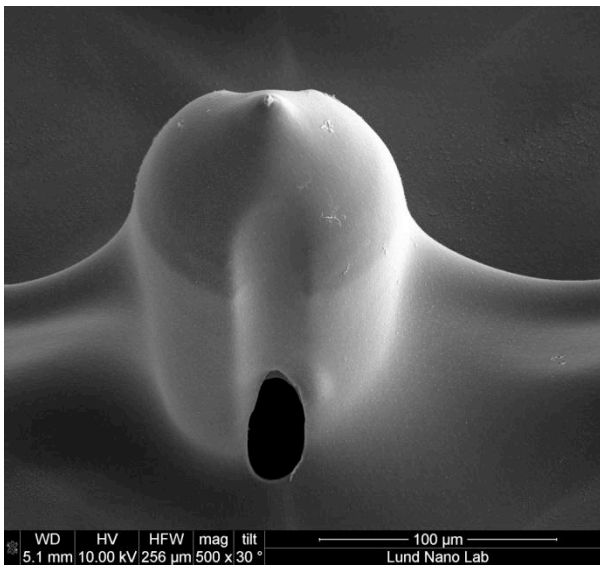
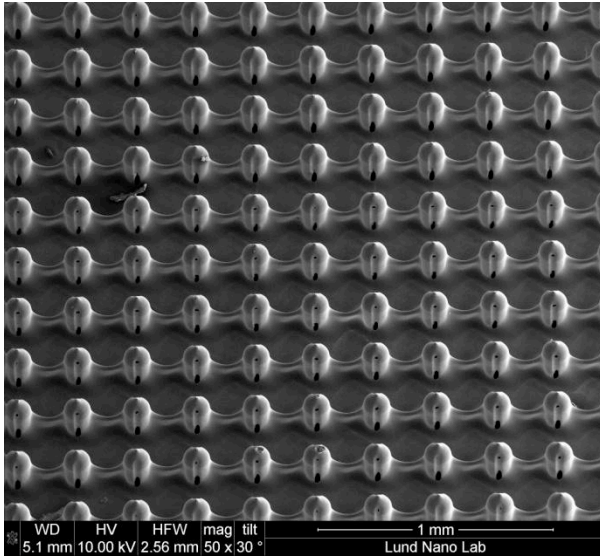


Figure 11| The silicon microneedle array is used to physically disrupt the dead corneocytes of the stratum corneum barrier. The 5 μm thick nanostructured thin film is sealed onto the microneedle array using vacuum suction and heat. The microneedles are 180 μm long and 120 μm in diameter, small enough to not interact with nerve endings. At the base of each microneedle, there are two holes where the drug enters from the above payload.

3.3 RESULTS & DISCUSSION

The *in vitro* results demonstrated that the nanostructured surfaces initiate active cellular processes to enable the transport of high molecular weight biologics across an

epithelial monolayer by loosening the tight junction proteins in the paracellular space. This continuous route of transport lends itself to drug delivery applications where the biologic must transport across stratified epithelial tissues such as the skin^{55,77}. To this end, a nanostructured surface was integrated into a microneedle transdermal patch for epidermal *in vivo* studies in a rabbit model. The microneedles provide a minimally invasive device that enables placement of the nanostructured surfaces in contact with viable epithelial cells by bypassing the dead corneocytes of the stratum corneum. The microneedle devices were constructed by draping a 5 μm thick nanostructured film over the microneedles and then using a combination of heat and vacuum to mold the film to the microneedle surfaces. Holes in the film at the microneedle tip allow drug transfer from the device reservoir to the nanostructure-cell interface (See Figure 11).

The nanostructured microneedle patches measured 25 mm by 25 mm with a density of 784 microneedles/ cm^2 , and were placed in intimate contact with the flank region of New Zealand White rabbits. Each needle was 300 microns tall and 100 microns in diameter and had side channels for transporting the drug from the reservoir to the nanostructure-cell interface through capillary forces. The study consisted of 3 groups: a subcutaneous injection group receiving 2.5 mg/animal (n=2), (2) the P(0.5, 1.4, 3.4) wrapped microneedles group receiving 1.875 mg/animal (n=5) and (3) the unstructured microneedles group receiving 1.875 mg/animal (n=4). At different time points over the 48 hour study, blood serum samples were collected and an ELISA assay was used to measure the etanercept concentration for the pharmacokinetic (PK) curves. At the end of the 48 hour study, the organ distribution of etanercept in the animals was also measured.

The in vivo results are presented in Figure 12. The pharmacokinetic curves show that the nanostructured microneedles significantly increased the absorption of etanercept versus the unstructured microneedles. There is a 90% increase in the maximum concentration (C_{max}) due to the nanostructured topography. Additionally, the bioavailability of the nanostructured microneedles is approximately 35 times greater than the unstructured microneedles. The bioavailability was calculated using Equation (1), where MN denotes microneedle, $SubQ$ denotes subcutaneous injection, and AUC denotes the area under the PK curve,

$$Bioavailability = \frac{AUC_{MN}}{AUC_{SubQ}} \times \frac{Dose_{SubQ}}{Dose_{MN}} \quad (1)$$

Furthermore, the organ distribution of etanercept was measured at 72 hours and the results are given in Figure 12b. In the animals treated with the nanostructured-microneedle patches, the etanercept concentrations were undetectable by the ELISA assay (<0.6 pg/mL) in the lymph node, liver, pancreas, spleen, and lung, and were only present in the kidney and bone marrow. In contrast, etanercept was detected in all the organs listed above for the animals treated with the subcutaneous injection, and it reached all the organs except the pancreas and the lung for the animals treated with the unstructured microneedles. Both the PK curves and organ distributions suggest that the nanostructured microneedles increase drug uptake by the bloodstream and minimize absorption by the lymphatic system. This is a significant change in the accepted perception that biologics with molecular weights larger than approximately 17.5 kDa are absorbed primarily through the lymphatic system^{78,79}. The observed change in the

transport phenomena is believed to result from the enhanced active transport mechanism as seen in the *in vitro* experiments with epithelial monolayers.

It is still not well understood how the nanostructure interactions permeate through epithelial tissue, however, it is well known that cells do transmit signals across cells⁸⁰. Studies have shown that a mechanical perturbation of a cell results in a wave of intracellular calcium ions (Ca^{2+}) that propagates from cell to cell through gap junctions up to 10-20 cells away from the local stimulus⁸¹. This Ca^{2+} wave triggered from the mechanical stimulus of the nanostructured surfaces may serve to coordinate a multicellular response. Numerous studies in the literature have reported that an increase in intracellular Ca^{2+} in epithelial cells results in a decrease in transepithelial electrical resistance, corresponding to a loosening in tight junction barrier function which could change tight junction morphology as we observed^{80,82}

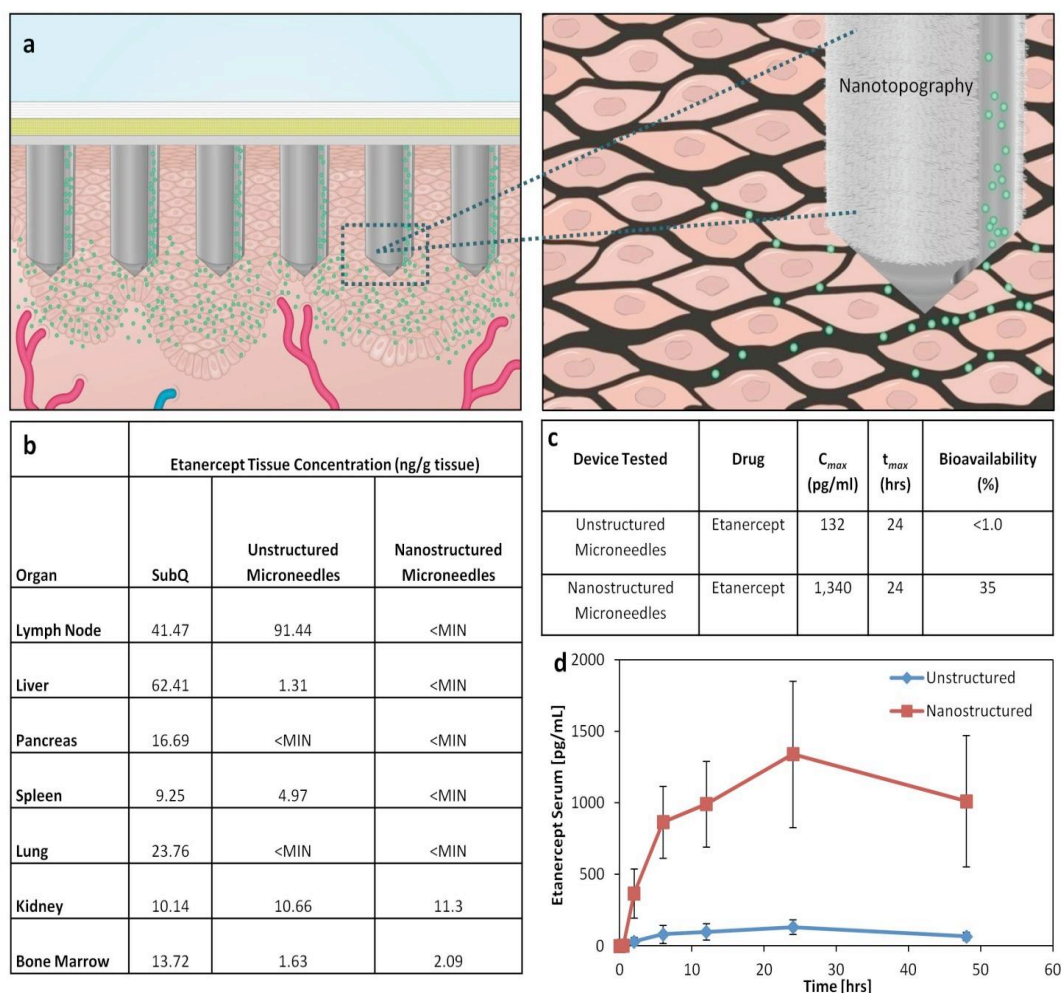


Figure 12| *In vivo* transdermal study. A schematic of the microneedle patch used for the transdermal *in vivo* studies is presented in a. The organ distribution of etanercept in the different organs of the rabbit is displayed in b and shows that absorption occurs primarily through the blood stream with minimal lymphatic uptake for the nanostructured microneedle patch. In contrast, the unstructured microneedles and subcutaneous injection led to significant lymphatic absorption. The bioavailability of the nanostructured devices was 35 times greater than that of the unstructured devices as shown in c. The serum concentration of etanercept (mean \pm SE) in the rabbits following the application of etanercept-loaded nanostructured microneedle patches and unstructured microneedle patches is shown in d.

The *in vitro* and *in vivo* results presented are the first demonstration of enhanced drug transport of high molecular weight biologics using nanotopographical cues. This novel strategy was proven in two different epithelial systems: the gastrointestinal system as modeled by Caco-2 cells and the stratified epithelium in skin as modeled by the *in vivo*

animal studies. The observed reduction in lymphatic uptake is a remarkable result because it suggests increased bioavailability and drug targeting for many poorly absorbable drugs. Additionally, the ability to increase permeability in tightly connected tissue could be used to increase drug penetration in tumors. We believe that by highlighting this enabling strategy of nanostructure-mediated transport, new light will be shed on the field of drug delivery by leveraging the natural biology of cells to improve drug efficacy and delivery of high potential biologics.

Chapter 4:

Nanostructured Surfaces as an Anti-Fibrotic Environment

Influencing cellular responses to biomaterials is crucial in the field of tissue engineering and regenerative medicine. Since cells are surrounded by extracellular matrix features that are on the nanoscale, identifying nanostructures for imparting desirable cellular function could greatly impact the field. Due to the rise in micro and nanofabrication techniques borrowed from the advances in the microelectronics industry, previously unattainable nanostructured surfaces on a variety of biomaterials can be generated. We investigated how nanostructured surfaces with varying nanofeature aspect ratios can influence the fibrotic response. The nanostructured surfaces with aspect ratio features greater than 5 induced less protein adsorption which led to rounded fibroblast morphologies. These nanofeatures also induced significantly lower gene expression of collagen 1 α 2, collagen 3 α 1, and growth factors related to fibroblast proliferation. The results demonstrate that well controlled nanostructured surfaces could be used as an anti-fibrotic environment for various medical applications such as implant or biosensor coatings.

4.1 BACKGROUND

Implant-induced fibrosis has generated much attention in the medical community and in the field of tissue engineering. Almost all soft tissue implants undergo fibrotic encapsulation and the eventual loss of functional tissue surrounding the implant. The

fibroblast is a specific cell that synthesizes and deposits extracellular matrix. The overproliferation of fibroblasts and the overproduction of extracellular matrix proteins has been implicated in fibrosis. Although much progress has been made in the biomaterials field, it is well known that implant fibrosis and encapsulation can often contribute to medical device failures. For example, fibrosis contributes to breast implant contracture as well as biosensor inactivation⁸³⁻⁸⁵. Fibrosis has also been implicated in post-surgical adhesions, contributing to the failure of gastrointestinal, gynecological and sinus surgeries⁸⁶.

To decrease fibrotic encapsulation around implants, new biomaterials need to be developed that foster an anti-fibrotic environment. There has been considerable work in the literature on chemistry-based approaches to decreasing fibrosis. For example, Risbud et. al and others reported how biocompatible hydrogels composed of chitosan-pyrrolidone arrest capsular fibroblast growth⁸⁷. Other materials such as alginate, hyaluronic acid, and derivatives of chitin have been shown to mimic fetal wound healing by selectively inhibiting fibroblast growth^{88,89}. Recently however, it has been established that cells are capable of responding to environmental topographical cues. The extracellular matrix is composed of complex architectural features at the nanoscale, including pores, fibers ridges, and protein band periodicities of approximately 60 nm⁴⁵. Microscale features, being on the same order of magnitude as the cells themselves, can influence cellular behavior by obstacle confinement with a relatively low resolution of control. However, nanoscale features being much smaller than the cell, have the ability to influence cells through more subtle cues. For example, recent biomimetic studies have shown that extracellular matrix topography influences cellular behaviors such as

morphology, proliferation, and differentiation⁹⁰⁻⁹². Therefore, nanotopography offers the opportunity to perturb a wide range of cellular responses compared to microtopography. A better understanding of the cell-material interface on the nanoscale enables the exploration of a spectrum of interactions that are crucial to designing advanced medical devices and implants.

To investigate how architecture influences cellular behavior, nanostructures must be fabricated with a high level of repeatability and precision. Current advancements in nano- and microtechnology offer new possibilities of probing cell-material interactions to better understand biological function^{93,94}. Ranging from microcontact printing to photolithography, there are numerous techniques for controlling the topographical features in a systematic way. One such fabrication technique to achieve nanofeatures is through nanoimprint lithography (NIL). This technique is a stamping process capable of generating nanometer scale patterns as small as 10 to 25 nm^{3,95}. In contrast to conventional photolithography, nanofeatures are generated by the direct mechanical deformation of a thermoplastic material using a mold with nanofeatures. The molds are fabricated using electron-beam lithography to overcome the diffraction limit of light and to produce features on the nanoscale. Here, we utilize NIL to generate various nanostructured surfaces as a platform to examine how nanostructural cues influence fibroblast behavior. Specifically, we hypothesized that certain nanostructured topographies influence protein adsorption leading to less fibroblast spreading, potentially providing a way to decrease fibrosis for implant coating applications.

4.2 MATERIALS & METHODS

Fabrication of Nanostructured Films

Molds for NIL were generated using the JEOL JBX-9300FS EBL System followed by selective reactive ion etching. The molds were stamped into FDA-approved polypropylene (Premier Lab Supply Inc., 25.4 mm) and polystyrene thin films (Plastic Suppliers Inc., 50.8 mm). The polymer thin films were placed in contact with the nanostructured molds and exposed to a temperature of 170°C and a pressure above the elastic modulus of the polymer films using an Obducat 6-inch nanoimprint lithography system. Afterwards, the mold was removed, resulting in well-defined nanofeatures.

Culture of cells on topographic nanostructured surfaces

NIH 3T3 mouse fibroblasts were cultured in DMEM high glucose supplemented with 10% fetal bovine serum and 1% penicillin/streptomycin. The cultures were incubated in an atmosphere containing 5% CO₂ and 90% relative humidity at 37°C. The cells were subcultured at 90% confluency by trypsinization with 0.25% trypsin-EDTA. Cells from passage numbers between 160 and 170 were used for the experiments.

Protein adsorption to nanostructured surfaces

Nanostructured thin films were cut into circular shapes with a 3 mm diameter biopsy punch and glued in place onto the bottom of a 24 well plate. After the glue dried, the thin films were thoroughly cleaned with 70% ethanol, followed by DI water overnight, and dried with compressed air. Solutions of FITC-IgG, FITC-BSA, and fibrinogen-Alexa Fluor 568 (all in 0.1 mg/mL) were incubated on the nanostructured surface for 2 hours. The thin films were rinsed with DI water and sonicated for 10 minutes. Finally, they were mounted for visualization with spinning disk confocal microscopy.

Contact angle measurements

Water contact angle measurements were performed with a goniometer to measure the wettability of the nanostructured surfaces. The nanostructured surfaces were thoroughly cleaned in a 99% isopropyl alcohol (IPA) bath and then fully dried. A single drop of DI water was placed on each nanostructured surface. The contact angle of the water droplet was measured by fitting a mathematical expression to the shape of the drop and then calculating the slope of the tangent to the drop at the liquid-solid-vapor (LSV) interface line.

Immunofluorescence staining of F-actin and Cell Area Quantification

Cells were fixed in 3.7% paraformaldehyde for 15 minutes and permeabilized with Triton X (0.1%) for 20 minutes. The F-Actin was stained with Phalloidin conjugated to Alexa Fluor 568 and diluted 1:40 in PBS for 30 minutes at 25°C. The nucleus was stained with Hoechst at a dilution of 1:2000 for 30 minutes. Samples were thoroughly washed 3 times with PBS and mounted on a glass cover slip with Vecta Shield before inspection with spinning disk confocal microscopy. Cells were detected through automated detection of the cell outline after thresholding the intensities. The image analysis software was downloaded from the National Institute of Health (USA) (Image J, <http://rsb.info.nih.gov/ij/>).

Cyquant Proliferation Assay

6 mm biopsy punches were used to cut the nanostructured thin films into a circular shape. The thin films were then glued to the bottom of the wells of 96-well plates. The films were sterilized with 70% Ethanol overnight and air-dried in the sterile cell culture hood. Fibroblasts were seeded at a density of 2000 cells per well and cultured over a 4

day time period. At different time points, the media was aspirated and the plate was frozen at -80°C overnight. A cell pellet of known cell number was used for a standard for quantifying cell number. The green-fluorescent Cyquant dye was used to detect the number of cells for each time point. The signal was read on a fluorometer at 495 nm.

Scanning electron microscopy

Fibroblasts were seeded onto the nanostructured thin films, and on day 2, they were fixed with 3% glutaraldehyde in 0.1 M sodium cacodylate (pH 7.4), containing 0.1M sucrose. After 45 minutes of incubation, the cells were rinsed with cacodylate-sucrose buffer for 10 minutes. Next, the samples were dehydrated by gently adding solutions of ethanol in a graded series of concentrations (35%, 50%, 75%, 95%, 100%, 100%) for 10 minutes each. The last step was to replace the 100% ethanol solution with HMDS, and then air dried in the fume hood for 30 minutes. The samples were then sputter coated with 200 Angstroms of gold-palladium.

qPCR Methods

3T3 cells were seeded at a density of 5000 cells/cm² in a 96-well tissue culture plate. The following films were placed in contact with the cells for 72 hours at 37°C: S(0.5, 1.4, 3.4), P(120), or P(flat). Cell lysis, reverse transcription, and qPCR (*Applied Biosystems, StepONEPlus*) were performed using the Fast SYBR Green cells to C_T kit in accordance with the manufacturer's instructions. The experiment was carried out in triplicate (n=3) and the evaluation of mRNA expression by qPCR was also run in triplicate. The expression of GAPDH, collagen type 1 alpha 2, collagen type 3 alpha 1, connective tissue growth factor (CTGF), epidermal growth factor (EGF), integrin linked kinase, and TGF

beta 1 were analyzed. The following primer pairs were used: GAPDH forward 5' - 3', GAPDH reverse 5' - 3'. The real time PCR results were analyzed using the $\Delta\Delta C_t$ method and normalized to GAPDH transcript levels.

Statistical Analysis

Data are reported as mean values +/- standard deviation. Multiple comparisons were analyzed with a one-way ANOVA test followed by the Holm t-test. P-values of less than 0.05 were considered statistically significant.

4.3 RESULTS

Nanoimprint lithography was utilized to generate 4 different unique nanostructured topographies as shown in Figure 1. The different substrates consisted of: a polypropylene film with high aspect ratio nanopillars (H = 16 μm , D = 800 nm, AR = 20, surface roughness = 850 nm); a polystyrene film with nanopillars (H = 1 μm , D = 200 nm, AR = 5, surface roughness = 73 nm); a polystyrene film with a patch-work pattern of nanostructures (H = 175 nm, D = 200 nm, AR = 0.88, surface roughness = 50 nm); and finally, a polystyrene film with 3 different nanopillars combined in a fractal pattern with the largest pillar diameter of 1 μm having an average height of 520 nm, the medium pillar diameter of 400 nm having an average height of 560 nm, and the smallest pillar diameter of 200 nm having an average height of 680 nm. The AR ratios for the three structures were 0.5, 1.4, and 3.4, and the average surface roughness was 145 nm. All films will be referred to as either P or S for polypropylene or polystyrene respectively, followed by the nanostructure aspect ratio in parentheses (e.g. "P(20)" encodes for the polypropylene film with a nanostructure aspect ratio of 20).

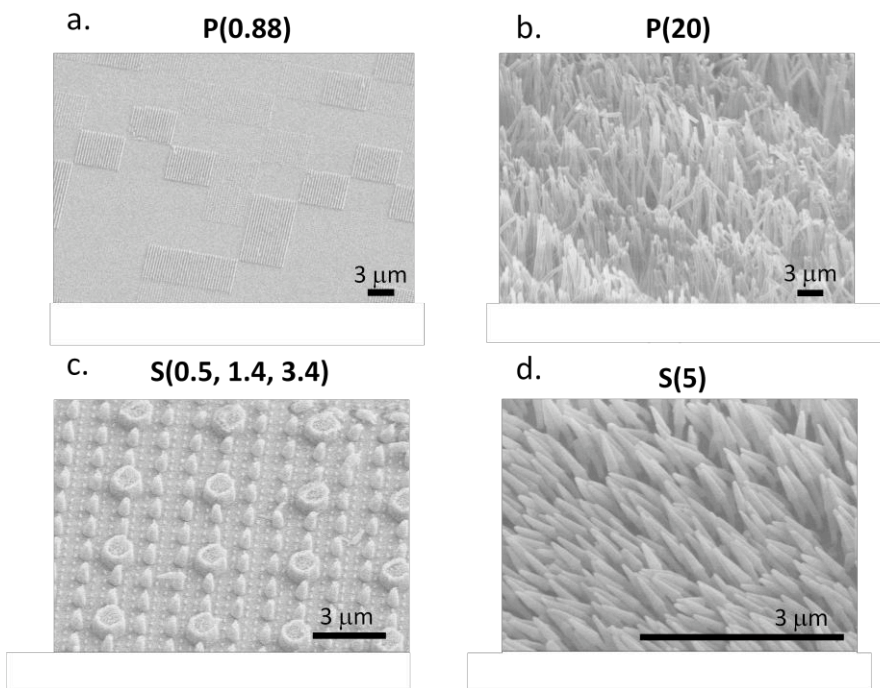


Figure 13| Scanning electron microscopy images of the nanostructured surfaces that were fabricated with nanoimprint lithography. a) and b) are made from polypropylene thin films as indicated by the "P," while c) and d) are fabricated from polystyrene thin films, as indicated by the "S." The numbers in parentheses represent the average aspect ratios of the nanostructures.

Characterization of the various surface energies was performed through static water contact angle measurements. Figure 14 shows the contact angles in degrees for each nanostructured substrate. P(20) resulted in a higher contact angle than that of the P(flat) control. Similarly, the polystyrene nanostructured S(5), S(0.5, 1.4, 3.4), and S(0.88) resulted in higher contact angles than the S(flat) control. These results indicate that regardless of material chemistry, the nanotopography increases the contact angles and therefore hydrophobicity of the thin films.

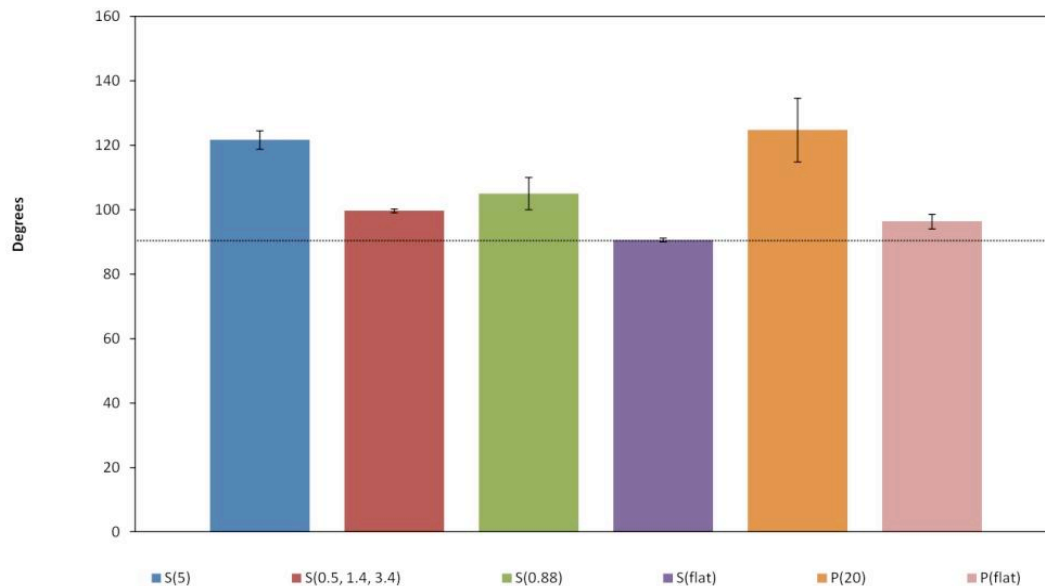


Figure 14| Contact angle measurements reveal that the nanotopography leads to higher contact angles (degrees) than the respective flat, unimprinted films of the same material chemistry.

Protein adsorption to surfaces is a complex process, which is driven by different protein-surface forces such as Van der Waals, hydrophobic/hydrophilic, and electrostatic interactions. Among these different parameters, the increased hydrophobicity of the nanostructured surfaces will strongly influence the amount of protein adsorption. To test this hypothesis, we incubated the nanostructured substrates in different protein solutions (FITC-BSA, FITC-IgG, and Alexa Fluor 568-Fibrinogen) and imaged them with confocal microscopy as shown in Figure 15. The nanotopography dramatically affects the way proteins adsorb to the different surfaces. For example, the higher aspect ratio features (S(5) and P(20)) seem to adsorb FITC-BSA, FITC-IgG, and fibrinogen to the tips of the nanopillars. In contrast, FITC-BSA and FITC-IgG adsorb to the tops of the micron-sized feature as well as the nanopillar tips of the hierarchical S(0.5, 1.4, 3.4) nanostructured thin film. However, fibrinogen appears to adsorb non-preferentially on the S(0.5, 1.4, 2.4)

surface. Furthermore, the heterogeneously patterned S(0.88) surface induced preferential protein adsorption in a quilt-like pattern for all three proteins.

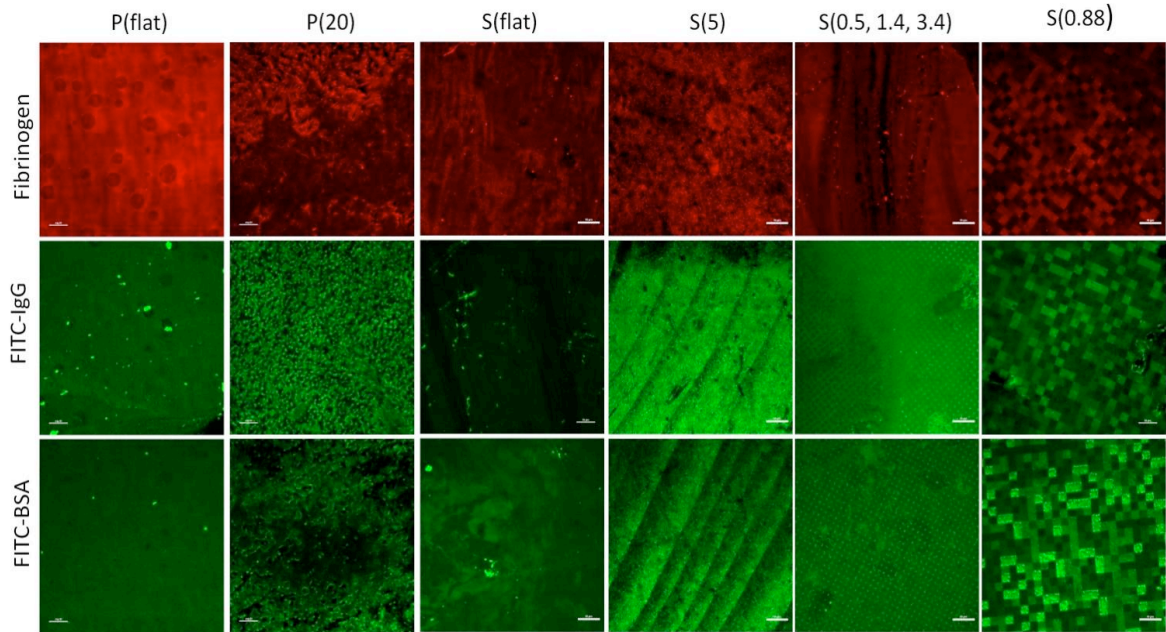


Figure 15| Protein adsorption onto the various nanostructured surfaces reveals that the underlying nanotopography greatly impacts the patterning of protein adsorption. It appears that the nanostructures with higher aspect ratios (P(20), S(5)) induce protein adsorption that is localized to the tips of the nanopillars. These higher aspect ratios repel proteins due to entropic repulsion and steric hindrance effects. Scale bar is 20 μ m.

The different protein adsorption patterns that we observed may strongly influence the growth of fibroblasts. Fibroblasts were cultured on the nanostructured substrates for 4 days and measured with the Cyquant cell proliferation assay at different time points to generate a cell proliferation curve. Figure 16 shows that fibroblasts grown on P(20) and S(5), the substrates with the highest aspect ratio features, seem to grow at the slowest rate. Additionally, observation of f-actin in the immunofluorescence staining showed different cell morphologies on the nanostructured surfaces compared to flat controls. As presented in Figure 5, the fibroblasts were well spread with many stress fibers on the

control flat substrates. However, the fibroblasts grown on P(20) and S(5) substrates, were less spread with fewer stress fibers. Quantitative analysis of cell morphology confirmed what was observed qualitatively. As the aspect ratio and surface roughness increases, the cellular area decreases.

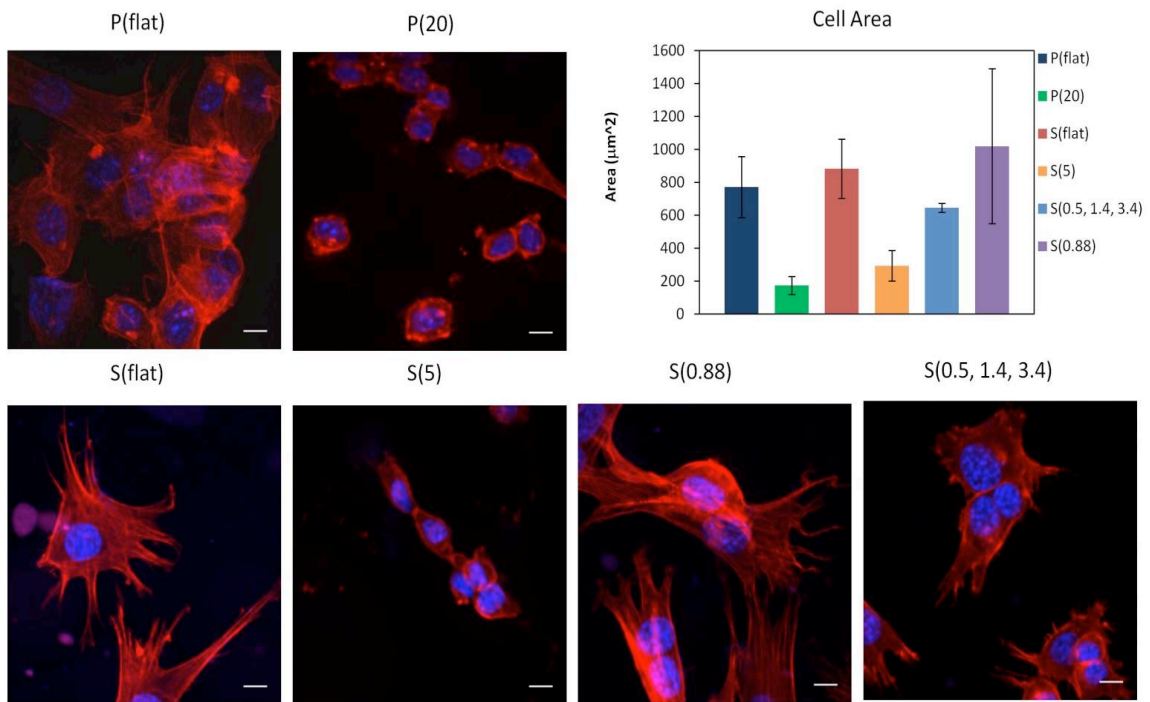


Figure 16| 3T3 fibroblasts were grown on the nanostructured thin films and stained with phalloidin that binds F-actin in red and with DAPI in blue. The two films with the higher aspect ratios (P(20), and S(5)) induce a rounded fibroblast morphology. The films that have lower aspect ratios have similar spread-out morphologies to the unimprinted control surfaces.

SEM was employed to directly image the interactions of the filopodia projections with the nanostructures. It is apparent that the shape of the nanostructure strongly influences the cell morphologies as shown in Figure 6. For example, fibroblasts seem to form adhesions

to the tips of the nanostructures in the S(0.5, 1.4, 3.4) substrate. Fibroblasts growing on the S(0.88) substrates appear to preferentially grow on certain nano-patterned features. The fibroblast in Figure 5 exhibits star-like filopodial projections that adhere to the nano-patterned square. Interestingly, these projections appear to terminate on the nanostructure patches that induced more concentrated protein adsorption. In contrast, fibroblasts appear to take on a rounded morphology on P(20) and S(5). The cells are "pinned" on top of the nanopillars and are unable to spread out as they do on the flat control surfaces.

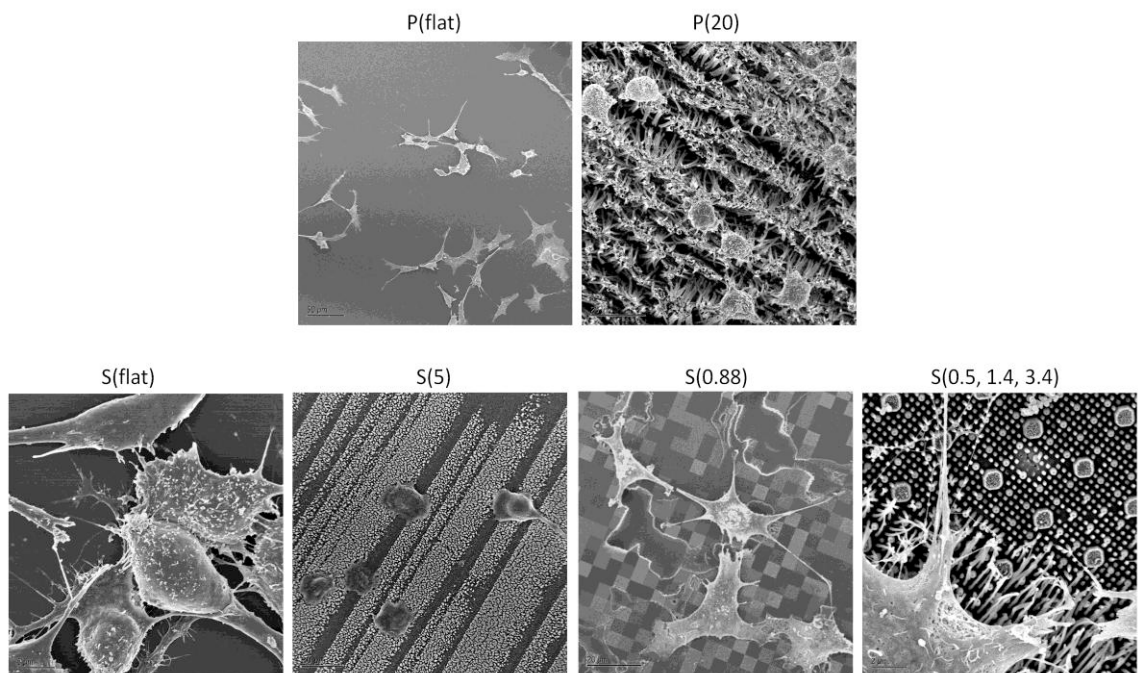


Figure 17| Scanning electron microscopy images of fibroblasts interacting directly with the nanostructures. Similar to Figure 4, P(20) and S(5) lead to rounded fibroblast morphologies, suggesting that these surfaces induce an anti-fibrotic environment.

We also investigated whether nanotopographical cues could cause alterations in the production of different markers involved in scar formation. Gene expression studies were performed to measure the transcription level of collagen 1 α 2 (COL1 α 2), collagen 3 α 1

(COL3 α 1), connective tissue growth factor (CTGF), Integrin linked kinase (ILK), tissue growth factor beta 1 (TGF β 1), and epidermal growth factor (EGF). Expression of these 6 genes was measured by qPCR. The results indicate that P(20) fosters a much more anti-fibrotic environment as shown in Figure 7. For example, both COL1A2 and COL3A1 are down regulated compared to the unimprinted and untreated controls. This finding translates into decreased collagen production and potentially reduced scarring *in vivo*. Similarly, CTGF, TGF β 1 and EGF, growth factors responsible for the proliferative behavior of fibroblasts, are significantly down regulated in the presence of the P(20) nanostructured surface. In contrast, there were no significant differences in transcription levels of these genes when fibroblasts were cultured on S(0.5, 1.4, 3.4). This nanostructured surface had a more heterogeneous surface with features having relatively low aspect ratios compared to the P(20). These gene expression results suggest that nanostructures with higher aspect ratios than 5 reduce fibroblast proliferation and ECM production which may ultimately translate into reduced scarring.

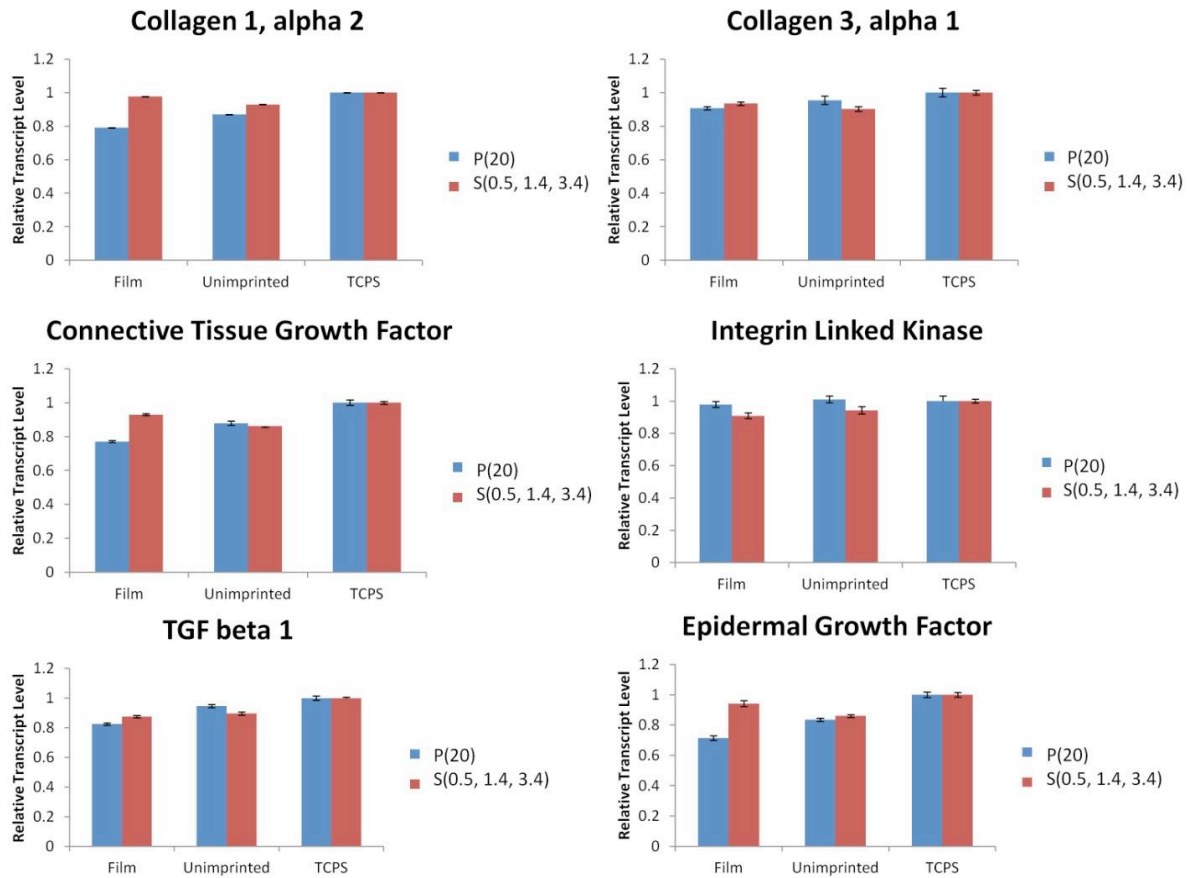


Figure 18| qPCR reveal that the nanostructures with the highest aspect ratio, P(20), lead to lower gene expression of collagen 1, alpha 2, collagen 3, alpha 1, connective tissue growth factor, integrin linked kinase, TGF beta 1, and epidermal growth factor. However, S(0.5, 1.4, 3.4) with relatively lower aspect ratios lead to higher gene expression levels than to that of P(20).

4.4 DISCUSSION

The extracellular matrix is a hierarchical environment containing microscale to nanoscale features ranging from tens of nanometers in length. Fibroblasts in a wound site interact with clusters of severed collagen fibrils in an inhomogeneous pattern, and they may perceive this environment as surfaces containing nano and micro grooves, ridges, and pillars with variable densities and roughness. Therefore, we attempted to recreate

these topographies in order to investigate the effects of nanostructural cues on fibroblast behavior.

In this study, we demonstrated how nanotopographical cues elicit a dramatic effect on cell shape, proliferation, and gene expression, with potential applications for decreasing scarring *in vivo*. We tested 4 different nanostructured surfaces and discovered that the ones with the highest aspect ratio features fostered an anti-fibrotic environment. This result may be directly related to the surface nanotopography or indirectly related to the way the surface topography influences extracellular matrix protein recruitment. The longer and thinner nanofeatures may resist protein adsorption due to steric hindrance and entropic repulsive forces⁹⁶. Although others have observed differential cellular responses to nanotopography, most have focused on cell-surface interactions and have not investigated the intermediate effect that nanostructures have on protein adsorption^{90,91,97-99}. Unlike microtopography whereby the cells are mechanically contained between features, nanotopography appears to work by influencing how proteins are presented to cells. The adsorption of proteins to biomaterial surfaces is a dynamic process whereby proteins bind, rearrange, and detach. This process plays a crucial role in determining cell growth, proliferation, and the overall incorporation of the biomaterial into the body. Depending on the nanofeature shape, the new surface energy may result in a more hydrophilic or hydrophobic environment, which can lead to protein resistance or even protein denaturation in the extreme case. P(20) and S(5) both have higher contact angles compared to the other surfaces. Perhaps this nanostructured superhydrophobic effect may cause protein conformational changes, ultimately affecting the cell-materials

interactions¹⁰⁰. Without suitable protein presentation on the surface, cells are less capable of adhering¹⁰¹.

The nanotopographies of the surfaces may contribute to the various fibroblast morphologies that were observed in Figure 17. Interestingly, fibroblasts grown on P(20) and S(5) exhibited more rounded morphologies as seen through the immunofluorescence and SEM studies. In contrast, cells grown on S(0.5, 1.4, 3.4), S(0.88), and the flat control surfaces exhibited more spread-out morphologies as quantified by higher cell area measurement. Numerous studies in the literature have described a common trend of decreased cellular adhesion and spreading with an increase in nanofeature height^{102,103}. This phenomenon is thought to be associated with perturbed focal adhesion formation as well as an inhibition of protein adsorption. In our studies, we observed differential protein adsorption patterns on the various surfaces. The nanostructures that induced rounded cellular morphologies also had protein adsorption localized only to the tips of the nanopillars. This would suggest that the cellular filopodia could not find suitable sites of attachment due to the reduced protein adsorption on the tips. Furthermore, this would indicate that the higher aspect ratio nanofeatures restrict integrin adhesion formation to the apexes of the nanopillars.

The SEM images reveal that nanoscale topographical features influence cellular spreading and focal adhesion formation. In Figure 18, it is apparent that the low aspect ratio nanofeatures promote more interaction with the cells. For example, S(0.5, 1.4, 3.4) has relatively low aspect ratio features, and we observed filopodia projections extending to the tips of the nanopillars. Filopodia tips are approximately 100 nm and are the main sensory tools for spatial information. Since the S(0.5, 1.4, 3.4) nanostructures have larger

diameters that range from 200 nm to 1 μm , the fibroblasts were able to form intact focal adhesions to this surface⁷. Similarly, S(0.88) is another nanostructured surface with low aspect ratio features. Fibroblasts on this surface were well spread, and each filopodia appears to be terminating on a region that has a high protein density. In contrast, it is apparent that the fibroblasts on P(20) and S(5) are pinned to the top of the nanopillars and unable to spread. Taken together, our observations are consistent with the well-established fact that anchorage-dependent cells must attach and spread on an underlying substrate in order to grow.

Since focal adhesions link the cytoskeleton to the ECM through integrin clustering, it was hypothesized that the ability of the fibroblast to adhere and spread will alter cell signaling and mechanotransduction processes. A potential explanation for the observed nanotopographical effects on fibroblast behavior could be the model of tensional integrity (tensegrity) developed by Ingber et. al in 1993⁷⁰. In this model, integrins act as mechanoreceptors that transmit mechanical signals through the tensionally integrated cytoskeleton. Therefore, those nanostructured surfaces that induce fewer and weaker focal adhesions may be associated with lower ECM production and gene expression since the reduced tension will lead to lower signal transduction to the nucleus⁷². Consistent with this hypothesis, P(20), the nanostructure with the highest aspect ratio features, induced lower gene expression levels for COL1A2, COL3A1, CTGF, TGF- β , and EGF compared to the controls. This decreased gene expression is in agreement with the significant reduction of cell growth observed on the same surface. COL1A2 and COL3A1 are significant components of scar tissue, so a down regulation in these genes suggests that this nanostructured surface would encourage an anti-fibrotic

environment.

CONCLUSION

In summary, we have demonstrated that nanotopography influences fibroblast proliferation, gene expression, and cellular morphology compared to flat control surfaces of the same material chemistry. The observed effects are most likely due to the altered protein adsorption to the nanofeatures. The proposed mechanism is through decreased focal adhesion formation. This work has broad applications for medical device implant coatings to promote an anti-fibrotic environment for decreased scar formation.

REFERENCES

1. Ainslie, K. M., Kraning, C. M. & Desai, T. A. Microfabrication of an asymmetric, multi-layered microdevice for controlled release of orally delivered therapeutics. *Lab Chip* 8, 1042–1047 (2008).
2. Qin, D., Xia, Y. & Whitesides, G. M. Soft lithography for micro- and nanoscale patterning. *Nat Protoc* 5, 491–502 (2010).
3. Chou, S. Y., Krauss, P. R. & Renstrom, P. J. Imprint Lithography with 25-Nanometer Resolution. *Science* 272, 85–87 (1996).
4. Krauss, P. R. & Chou, S. Y. Sub-10 nm imprint lithography and applications. *1997 55th Annual Device Research Conference Digest* 90–91doi:10.1109/DRC.1997.612486
5. Odom, T. W., Love, J. C., Wolfe, D. B., Paul, K. E. & Whitesides, G. M. Improved Pattern Transfer in Soft Lithography Using Composite Stamps. *Langmuir* 18, 5314–5320 (2002).
6. Xia, Y. & Whitesides, G. M. Soft Lithography. *Angewandte Chemie International Edition* 37, 550–575 (1998).
7. Perry, J. L., Herlihy, K. P., Napier, M. E. & DeSimone, J. M. PRINT: A Novel Platform Toward Shape and Size Specific Nanoparticle Theranostics. *Acc. Chem. Res.* 44, 990–998 (2011).
8. Canelas, D. A., Herlihy, K. P. & DeSimone, J. M. Top-down particle fabrication: control of size and shape for diagnostic imaging and drug delivery. *Wiley Interdiscip Rev Nanomed Nanobiotechnol* 1, 391–404 (2009).

9. Champion, J. A. & Mitragotri, S. Role of target geometry in phagocytosis. *PNAS* 103, 4930–4934 (2006).
10. Hillery, A. M., Lloyd, A. W. & Swarbrick, J. *Drug Delivery and Targeting: For Pharmacists and Pharmaceutical Scientists*. (CRC Press: 2002).
11. Kitchens, K., Kolhatkar, R., Swaan, P., Eddington, N. & Ghandehari, H. Transport of Poly(Amidoamine) Dendrimers across Caco-2 Cell Monolayers: Influence of Size, Charge and Fluorescent Labeling. *Pharmaceutical Research* 23, 2818–2826 (2006).
12. Niessen, C. M. Tight Junctions/Adherens Junctions: Basic Structure and Function. *J Invest Dermatol* 127, 2525–2532 (0000).
13. Peppas, N. A. & Huang, Y. Nanoscale technology of mucoadhesive interactions. *Advanced Drug Delivery Reviews* 56, 1675–1687 (2004).
14. Baloglu, E., Senyigit, Z. A., Karavana, S. Y. & Bernkop-Schnürch, A. Strategies to prolong the intravaginal residence time of drug delivery systems. *J Pharm Pharm Sci* 12, 312–336 (2009).
15. Woodley, J. Bioadhesion - New possibilities for drug administration? *Clin. Pharmacokinet.* 40, 77–84 (2001).
16. Smart, J. D. Recent developments in the use of bioadhesive systems for delivery of drugs to the oral cavity. *Crit. Rev. Ther. Drug Carr. Syst.* 21, 319–344 (2004).
17. Uskoković, V., Lee, P. P., Walsh, L. A., Fischer, K. E. & Desai, T. A. PEGylated silicon nanowire coated silica microparticles for drug delivery across intestinal epithelium. *Biomaterials* 33, 1663–1672 (2012).
18. Fischer, K. E. *et al.* Biomimetic nanowire coatings for next generation adhesive drug delivery systems. *Nano Lett* 9, 716–720 (2009).

19. Fischer, K. E. *et al.* Hierarchical nanoengineered surfaces for enhanced cytoadhesion and drug delivery. *Biomaterials* 32, 3499–3506 (2011).
20. Autumn, K. *et al.* Evidence for van der Waals adhesion in gecko setae. *PNAS* 99, 12252–12256 (2002).
21. Izadi, H., Zhao, B., Han, Y., McManus, N. & Penlidis, A. Teflon hierarchical nanopillars with dry and wet adhesive properties. *J. Polym. Sci. Pt. B-Polym. Phys.* 50, 846–851 (2012).
22. Lee, H., Lee, B. P. & Messersmith, P. B. A reversible wet/dry adhesive inspired by mussels and geckos. *Nature* 448, 338–341 (2007).
23. Mahdavi, A. *et al.* A biodegradable and biocompatible gecko-inspired tissue adhesive. *Proceedings of the National Academy of Sciences* 105, 2307–2312 (2008).
24. Adriani, G. *et al.* The preferential targeting of the diseased microvasculature by disk-like particles. *Biomaterials* 33, 5504–5513 (2012).
25. McAllister, D. V., Allen, M. G. & Prausnitz, M. R. Microfabricated microneedles for gene and drug delivery. *Annu Rev Biomed Eng* 2, 289–313 (2000).
26. van der Maaden, K., Jiskoot, W. & Bouwstra, J. Microneedle technologies for (trans)dermal drug and vaccine delivery. *Journal of Controlled Release* 161, 645–655 (2012).
27. Mikszta, J. A. *et al.* Improved genetic immunization via micromechanical disruption of skin-barrier function and targeted epidermal delivery. *Nature Medicine* 8, 415–419 (2002).

28. McAllister, D. V. *et al.* Microfabricated needles for transdermal delivery of macromolecules and nanoparticles: Fabrication methods and transport studies. *PNAS* 100, 13755–13760 (2003).
29. Matsuo, K. *et al.* A low-invasive and effective transcutaneous immunization system using a novel dissolving microneedle array for soluble and particulate antigens. *J. Control. Release* 161, 10–17 (2012).
30. Chu, L. Y. & Prausnitz, M. R. Separable arrowhead microneedles. *Journal of Controlled Release* 149, 242–249 (2011).
31. Gratton, S. E. A. *et al.* The effect of particle design on cellular internalization pathways. *Proceedings of the National Academy of Sciences* 105, 11613 –11618 (2008).
32. Geng, Y. *et al.* Shape effects of filaments versus spherical particles in flow and drug delivery. *Nat Nano* 2, 249–255 (2007).
33. Sharma, G. *et al.* Polymer particle shape independently influences binding and internalization by macrophages. *J Control Release* 147, 408–412 (2010).
34. Li, X. Size and shape effects on receptor-mediated endocytosis of nanoparticles. *Journal of Applied Physics* 111, 024702–024702–4 (2012).
35. Teo, B. K. K. *et al.* The effect of micro and nanotopography on endocytosis in drug and gene delivery systems. *Biomaterials* 32, 9866–9875 (2011).
36. Bernards, D. A. & Desai, T. A. Nanotemplating of Biodegradable Polymer Membranes for Constant-Rate Drug Delivery. *Adv. Mater.* 22, 2358–2362 (2010).
37. He, H. *et al.* Use of a nanoporous biodegradable miniature device to regulate cytokine release for cancer treatment. *J. Control. Release* 151, 239–245 (2011).

38. Sahay, R. *et al.* Electrospun composite nanofibers and their multifaceted applications. *J. Mater. Chem.* **22**, 12953–12971 (2012).
39. Sundaramurthi, D., Vasanthan, K. S., Kuppan, P., Krishnan, U. M. & Sethuraman, S. Electrospun nanostructured chitosan–poly(vinyl alcohol) scaffolds: a biomimetic extracellular matrix as dermal substitute. *Biomedical Materials* **7**, 045005 (2012).
40. Rapoport, H. S. *et al.* Construction of a Tubular Scaffold that Mimics J-Shaped Stress/Strain Mechanics Using an Innovative Electrospinning Technique. *Tissue Eng. Part C-Methods* **18**, 567–574 (2012).
41. Jeffries, E. M. & Wang, Y. Biomimetic micropatterned multi-channel nerve guides by templated electrospinning. *Biotechnol. Bioeng.* **109**, 1571–1582 (2012).
42. Kurpinski, K. T., Stephenson, J. T., Janairo, R. R. R., Lee, H. & Li, S. The effect of fiber alignment and heparin coating on cell infiltration into nanofibrous PLLA scaffolds. *Biomaterials* **31**, 3536–3542 (2010).
43. Zhu, Y. *et al.* Engineering Bi-Layer Nanofibrous Conduits for Peripheral Nerve Regeneration. *Tissue Engineering Part C: Methods* **17**, 705–715 (2011).
44. Truskett, V. N. & Watts, M. P. C. Trends in imprint lithography for biological applications. *Trends in Biotechnology* **24**, 312–317 (2006).
45. Yim, E. K. F. *et al.* Nanopattern-induced changes in morphology and motility of smooth muscle cells. *Biomaterials* **26**, 5405–5413 (2005).
46. Hu, W., Yim, E. K. F., Reano, R. M., Leong, K. W. & Pang, S. W. Effects of nanoimprinted patterns in tissue-culture polystyrene on cell behavior. *J. Vac. Sci. Technol. B* **23**, 2984 (2005).

47. Johansson, F., Carlberg, P., Danielsen, N., Montelius, L. & Kanje, M. Axonal outgrowth on nano-imprinted patterns. *Biomaterials* 27, 1251–1258 (2006).
48. Cohen, A., Liu-Synder, P., Storey, D. & Webster, T. J. Decreased fibroblast and increased osteoblast functions on ionic plasma deposited nanostructured Ti coatings. *Nanoscale Res. Lett.* 2, 385–390 (2007).
49. Peng, L., Eltgroth, M. L., LaTempa, T. J., Grimes, C. A. & Desai, T. A. The effect of TiO₂ nanotubes on endothelial function and smooth muscle proliferation. *Biomaterials* 30, 1268–1272 (2009).
50. Prausnitz, M. R., Allen, M. G., Mcallister, D. V. & Henry, S. Microneedle device for transport of molecules across tissue. (2003).at <<http://www.freepatentsonline.com/6503231.html>>
51. Xia, H. *et al.* Low molecular weight protamine-functionalized nanoparticles for drug delivery to the brain after intranasal administration. *Biomaterials* 32, 9888–9898 (2011).
52. Oh, D.-H., Chun, K.-H., Jeon, S.-O., Kang, J.-W. & Lee, S. Enhanced transbuccal salmon calcitonin (sCT) delivery: Effect of chemical enhancers and electrical assistance on in vitro sCT buccal permeation. *Eur. J. Pharm. Biopharm.* 79, 357–363 (2011).
53. Gratieri, T., Gelfuso, G. M., de Freitas, O., Rocha, E. M. & Lopez, R. F. V. Enhancing and sustaining the topical ocular delivery of fluconazole using chitosan solution and poloxamer/chitosan in situ forming gel. *Eur. J. Pharm. Biopharm.* 79, 320–327 (2011).

54. Polat, B. E., Hart, D., Langer, R. & Blankschtein, D. Ultrasound-mediated transdermal drug delivery: Mechanisms, scope, and emerging trends. *J. Control. Release* 152, 330–348 (2011).
55. Sonaje, K. *et al.* Self-Assembled pH-Sensitive Nanoparticles: A Platform for Oral Delivery of Protein Drugs. *Adv. Funct. Mater.* 20, 3695–3700 (2010).
56. Shofner, J. P., Phillips, M. A. & Peppas, N. A. Cellular Evaluation of Synthesized Insulin/Transferrin Bioconjugates for Oral Insulin Delivery Using Intelligent Complexation Hydrogels. *Macromol. Biosci.* 10, 299–306 (2010).
57. Scheindlin, S. Transdermal Drug Delivery: PAST, PRESENT, FUTURE. *Molecular Interventions* 4, 308–312 (2004).
58. Goldie, R. *Immunopharmacology of epithelial barriers*. (Elsevier: 1994).
59. Doshi, N. & Mitragotri, S. Needle-shaped polymeric particles induce transient disruption of cell membranes. *Journal of The Royal Society Interface* 7, S403–S410 (2010).
60. Champion, J. A., Katare, Y. K. & Mitragotri, S. Particle shape: A new design parameter for micro- and nanoscale drug delivery carriers. *Journal of Controlled Release* 121, 3–9 (2007).
61. Dalby, M. J. Topographically induced direct cell mechanotransduction. *Med Eng Phys* 27, 730–742 (2005).
62. Dalby, M. J., Riehle, M. O., Sutherland, D. S., Agheli, H. & Curtis, A. S. G. Use of nanotopography to study mechanotransduction in fibroblasts--methods and perspectives. *Eur. J. Cell Biol.* 83, 159–169 (2004).

63. Magjarevic, R., Goldberg, D. S., Swaan, P. W. & Ghandehari, H. Mechanisms of Poly(amido amine) Dendrimer Transepithelial Transport and Tight Junction Modulation in Caco-2 Cells. *26th Southern Biomedical Engineering Conference SBEC 2010, April 30 - May 2, 2010, College Park, Maryland, USA* 32, 236–239 (2010).
64. Puckett, S., Pareta, R. & Webster, T. J. Nano rough micron patterned titanium for directing osteoblast morphology and adhesion. *Int J Nanomedicine* 3, 229–241 (2008).
65. Puckett, S. D., Lee, P. P., Ciombor, D. M., Aaron, R. K. & Webster, T. J. Nanotextured titanium surfaces for enhancing skin growth on transcutaneous osseointegrated devices. *Acta Biomaterialia* 6, 2352–2362 (2010).
66. Khang, D., Lu, J., Yao, C., Haberstroh, K. M. & Webster, T. J. The role of nanometer and sub-micron surface features on vascular and bone cell adhesion on titanium. *Biomaterials* 29, 970–983 (2008).
67. Yu, D. *et al.* MLCK-Dependent Exchange and Actin Binding Region-Dependent Anchoring of ZO-1 Regulate Tight Junction Barrier Function. *PNAS* 107, 8237–8241 (2010).
68. Shen, L. *et al.* Myosin Light Chain Phosphorylation Regulates Barrier Function by Remodeling Tight Junction Structure. *J Cell Sci* 119, 2095–2106 (2006).
69. Macia, E. *et al.* Dynasore, a Cell-Permeable Inhibitor of Dynamin. *Developmental Cell* 10, 839–850 (2006).
70. Wang, N., Butler, J. P. & Ingber, D. E. Mechanotransduction Across the Cell Surface and Through the Cytoskeleton. *Science* 260, 1124–1127 (1993).

71. McNeil, E., Capaldo, C. T. & Macara, I. G. Zonula occludens-1 function in the assembly of tight junctions in Madin-Darby canine kidney epithelial cells. *Mol. Biol. Cell* 17, 1922–1932 (2006).
72. Dalby, M. J. *et al.* Nanotopographical stimulation of mechanotransduction and changes in interphase centromere positioning. *Journal of Cellular Biochemistry* 100, 326–338 (2007).
73. Tian, Y. C. & Phillips, A. O. Interaction between the Transforming Growth Factor- β Type II Receptor/Smad Pathway and β -Catenin during Transforming Growth Factor- β 1-Mediated Adherens Junction Disassembly. *Am J Pathol* 160, 1619–1628 (2002).
74. Jin, M., Chen, Y., He, S., Ryan, S. J. & Hinton, D. R. Hepatocyte growth factor and its role in the pathogenesis of retinal detachment. *Invest. Ophthalmol. Vis. Sci.* 45, 323–329 (2004).
75. Wang, W., Dentler, W. L. & Borchardt, R. T. VEGF increases BMEC monolayer permeability by affecting occludin expression and tight junction assembly. *Am. J. Physiol. Heart Circ. Physiol.* 280, H434–440 (2001).
76. Gill, H. S. & Prausnitz, M. R. Coated microneedles for transdermal delivery. *J Control Release* 117, 227–237 (2007).
77. Baek, J.-S. *et al.* Alendronate-loaded microparticles for improvement of intestinal cellular absorption. *Journal of Drug Targeting* 19, 37–48 (2011).
78. Audus, K. L. & Raub, T. J. *Biological barriers to protein delivery.* (Springer: 1993).
79. Harvey, A. J. *et al.* Microneedle-based intradermal delivery enables rapid lymphatic uptake and distribution of protein drugs. *Pharm. Res.* 28, 107–116 (2011).

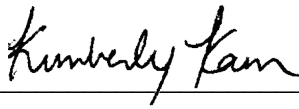
80. Sneyd, J., Wetton, B. T., Charles, A. C. & Sanderson, M. J. Intercellular calcium waves mediated by diffusion of inositol trisphosphate: a two-dimensional model. *American Journal of Physiology - Cell Physiology* 268, C1537–C1545 (1995).
81. Gonzalez-Mariscal, L. *et al.* Role of calcium in tight junction formation between epithelial cells. *American Journal of Physiology - Cell Physiology* 259, C978–C986 (1990).
82. Bhat, M. *et al.* Regulation of tight junction permeability by calcium mediators and cell cytoskeleton in rabbit tracheal epithelium. *Pharm. Res* 10, 991–997 (1993).
83. Chegini, N. Peritoneal molecular environment, adhesion formation and clinical implication. *Front. Biosci.* 7, e91–115 (2002).
84. Hunter, L. W., Lieske, J. C., Tran, N. V. & Miller, V. M. The association of matrix Gla protein isomers with calcification in capsules surrounding silicone breast implants. *Biomaterials* 32, 8364–8373 (2011).
85. Giurgiutiu, V. *et al.* Electromechanical impedance sensor for in vivo monitoring the body reaction to implants. *J Invest Surg* 17, 257–270 (2004).
86. Schippers, E., Tittel, A., Ottinger, A. & Schumpelick, V. Laparoscopy versus laparotomy: comparison of adhesion-formation after bowel resection in a canine model. *Dig Surg* 15, 145–147 (1998).
87. Risbud, M., Hardikar, A. & Bhonde, R. Growth modulation of fibroblasts by chitosan-polyvinyl pyrrolidone hydrogel: Implications for wound management? *J. Biosci.* 25, 25–31 (2000).

88. Li, Y., Rodrigues, J. & Tomas, H. Injectable and biodegradable hydrogels: gelation, biodegradation and biomedical applications. *Chem. Soc. Rev.* 41, 2193–2221 (2012).
89. Mast, B. A., Diegelmann, R. F., Krummel, T. M. & Cohen, I. K. Hyaluronic acid modulates proliferation, collagen and protein synthesis of cultured fetal fibroblasts. *Matrix* 13, 441–446 (1993).
90. Pennisi, C. P. *et al.* Nanoscale topography reduces fibroblast growth, focal adhesion size and migration-related gene expression on platinum surfaces. *Colloids and Surfaces B: Biointerfaces* 85, 189–197 (2011).
91. Kim, D.-H. *et al.* Mechanosensitivity of fibroblast cell shape and movement to anisotropic substratum topography gradients. *Biomaterials* 30, 5433–5444 (2009).
92. Karuri, N. W., Porri, T. J., Albrecht, R. M., Murphy, C. J. & Nealey, P. F. Nano- and microscale holes modulate cell-substrate adhesion, cytoskeletal organization, and α -beta1 integrin localization in SV40 human corneal epithelial cells. *IEEE Trans Nanobioscience* 5, 273–280 (2006).
93. Micro/nano-fabrication technologies for cell biology. *Med. Biol. Eng. Comput. (Germany)* 48, 1023–1032 (2010).
94. Lithographic microfabrication of biocompatible polymers for tissue engineering and lab-on-a-chip applications. *Proc. SPIE - Int. Soc. Opt. Eng. (USA)* 8427, 84271X (9 pp.)–84271X (9 pp.)84271X (9 pp.) (2012).
95. Chou, S. Y. & Krauss, P. R. Imprint lithography with sub-10 nm feature size and high throughput. *Microelectron. Eng.* 35, 237–240 (1997).

96. Rixman, M. A., Dean, D., Macias, C. E. & Ortiz, C. Nanoscale intermolecular interactions between human serum albumin and alkanethiol self-assembled monolayers. *Langmuir* 19, 6202–6218 (2003).
97. Wood, M. A., Bagnaninchi, P. & Dalby, M. J. The beta integrins and cytoskeletal nanoimprinting. *Exp. Cell Res.* 314, 927–935 (2008).
98. Dalby, M. J. Cellular response to low adhesion nanotopographies. *Int J Nanomedicine* 2, 373–381 (2007).
99. Dalby, M. J., Yarwood, S. J., Johnstone, H. J. ., Affrossman, S. & Riehle, M. O. Fibroblast signaling events in response to nanotopography: a gene array study. *IEEE Transactions on NanoBioscience* 1, 12–17 (2002).
100. Roach, P., Farrar, D. & Perry, C. C. Interpretation of Protein Adsorption: Surface-Induced Conformational Changes. *J. Am. Chem. Soc.* 127, 8168–8173 (2005).
101. Misra, R. D. K., Girase, B., Nune, V. K. C. & Xu, W. Cellular Interactions and Modulated Osteoblasts Functions Mediated by Protein Adsorption. *Adv. Eng. Mater.* 14, B247–B257 (2012).
102. Sjöström, T. *et al.* Fabrication of pillar-like titania nanostructures on titanium and their interactions with human skeletal stem cells. *Acta Biomater* 5, 1433–1441 (2009).
103. Lee, J., Chu, B. H., Chen, K.-H., Ren, F. & Lele, T. P. Randomly oriented, upright SiO₂ coated nanorods for reduced adhesion of mammalian cells. *Biomaterials* 30, 4488–4493 (2009).

PUBLISHING AGREEMENT

I hereby grant permission to the Graduate Division of the University of California, San Francisco to release copies of my thesis, dissertation, or manuscript to the Campus Library to provide access and preservation, in whole or in part, in perpetuity.



October 11th, 2012

Author Signature

Date